The CMB Power Spectrum and formation of structures in our Universe

Anton Brekke*
Theoretical Physics, University of Oslo
(Dated: June 6, 2024)

The Cosmic Microwave Background (CMB) radiation is a relic from the early universe, providing a snapshot of the cosmos approximately 380,000 years after the Big Bang. This faint glow, permeating the entire sky, holds valuable information about the composition and evolution of the Universe. Through the ΛCDM-model with initial values from [1], we develop an Einstein-Boltzmann solver to make a prediction of the CMB and matter power spectrum by considering linear perturbation theory on a flat FLRW universe as our background cosmology. Comparing our model to data from the supernova [2] we find that demanding a flat Universe forces us to include dark energy $\Omega_{\text{DE}} \sim 0.66 - 0.76$. We also predict the acceleration of the Universe to happen when $\Omega_\Lambda \approx \frac{1}{3}$. We also found that during recombination, the event of last scattering happened at time $t = 0.37801\,\text{Myr}$, as well as a freeze-out abundance $X_e(x = 0) = 2.02 \cdot 10^{-4}$ today. Finally, we obtain results for the power spectrums, giving us an esitimated theoretical upper bound $\lambda \approx 486\,\text{Mpc} = 1.62\,\text{Gly}$ for the size of cosmological structures. Comparing the power spectrums to data from [1], [3] and [4] we also find inaccuracies in our predicted model due to ignoring neutrinos, polarization and matter heavier than hydrogen.

CONTENTS

* https://github.com/AntonBrekke/AST5220; antonabr@uio.no

INTRODUCTION

This project is based on the code templates from GitHub, Hans A. Winther (2024), and most material is taken from the AST5220 course website [5].

The CMB serves as a crucial window into the early universe, offering insights into its composition and evolution. One of the most powerful tools for analyzing the CMB is the CMB power spectrum, which quantifies the temperature fluctuations of the CMB as a function of angular scale ℓ on the sky. This project thus focuses on the extraction and analysis of the CMB power spectrum, hopefully also projecting the CMB onto the sky. We develop an Einstein-Boltzmann solver that computes theoretical predictions for cosmological observables of the CMB and observations of the large structure of the Universe from galaxy surveys.

In the first Milestone, we start by introducing the ΛCDM-model to calculate our background cosmology. We do so by using the cosmological principle, getting a flat Friedmann-Robertson-Walker Universe. We then solve for the background cosmology by deriving the Friedmann-equations from the Einstein-equations, modelling all particle species as perfect fluids. We use data from [1] for initial values of cosmological parameters and [2] to predict a posterior value for H_0, as well as finding constraints on our Universe.

In the second Milestone, we solve for the recombination history of the Universe. This is important, as this is the epoch where the CMB becomes visible after photons decouple from baryons. We derive and use the Saha equation for fractional electron density in the early Universe, and also use the Peebles equation to solve for the remaining evolution. We also determine the event of last scattering, giving a rough estimate of when recombination happens.

In the third Milestone, we take into consideration that we have fluctuations in our spacetime background and matter densities by doing linear perturbation theory on the metric and densities. This is important, as a completely flat Universe would not give us any cosmological structures - which we most certainly have in our Universe. This leads us to solving a large set of coupled ODE's, giving perturbations of various quantities given in this Milestone. These fluctuations is essentially what gives us the fluctuations in the CMB we observe.

Finally, in the fourth and last Milestone, we calculate the CMB power spectrum, as well as the matter power spectrum. After discovering that solving the coupled ODE's for photon multipoles in Milestone 3 is rather heavy to solve, we develop a "new", rather elegant technique called line-of-sight integration to solve these. This allows us to quickly solve for the multipoles, and thus the power spectrums. We then compare our theoretical predictions to data from [1], [3], and [4].

1. MILESTONE I

In this Milestone we want to calculate the evolution of a homogeneous and isotropic universe. The main goal is to calculate relevant cosmological quantities, and compare this to observational data. The data we will use in this Milestone will be the data from Planck 2018 [1] and supernova data from Betoule [2].

1.1. Theory

1.1.1. ΛCDM-model

We start by assuming a homogeneous and isotropic universe. From this (and the Schwarszchild solution) we can derive the Friedmann-Robertson-Walker (FLRW) metric given as

$$ds^2 = -cdt^2 + a(t)^2(dx^2 + dy^2 + dz^2).$$

From the FLRW metric we can further derive the Friedmann-equations

$$\dot{\rho}_n + 3H(\rho_n + P_n) = 0,$$
$$H^2 = \frac{8\pi G}{3}\sum_n \rho_n$$

from the Einstein equation $G_{\mu\nu} = 8\pi G T_{\mu\nu}$ and conservation equation $\nabla_\mu T^{\mu\nu} = 0$ where ∇_μ is the covariant derivative. In the Friedmann-equations, ρ_n is the density, $H \equiv \dot{a}/a$ is the Hubble-factor, and P_n is the pressure. Using the Friedmann equations we can solve for density parameters Ω_n using the equation of state $\omega \equiv \rho/P = $ const. to relate density ρ_n and pressure P_n, which gives $\rho_n \propto a^{-3(1+\omega_n)}$ where $a = a(t)$ is the expansion coefficient. We write the density with a normalization constant s.t. $\rho_n = \rho_{n,0}a^{-3(1+\omega_n)}$. Defining the critical density $\rho_c = 3H_0^2/8\pi G$ (the value at which the Universe is at balance, and expansion is stopped) we simply get

$$\sum_n \frac{\rho_n}{\rho_c} \equiv \sum_n \Omega_n = 1 \tag{1}$$

where we define $\rho_n/\rho_c \equiv \Omega_n$. This then allows us to write

$$H^2 = \frac{8\pi G}{3}\sum_n \frac{\rho_{n,0}}{a^{3(1+\omega_n)}} = H_0^2 \sum_n \frac{\Omega_{n,0}}{a^{3(1+\omega_n)}}.$$

In the ΛCDM model we have the density parameters

$$\Omega_k(a) = \frac{\Omega_{k0}H_0^2}{a^2H(a)^2} \quad \text{(Curvature)} \tag{2}$$

$$\Omega_{\text{CDM}}(a) = \frac{\Omega_{\text{CDM0}}H_0^2}{a^3H(a)^2} \quad \text{(Cold Dark Matter)} \tag{3}$$

$$\Omega_b(a) = \frac{\Omega_{b0}H_0^2}{a^3H(a)^2} \quad \text{(Baryons)} \tag{4}$$

$$\Omega_\gamma(a) = \frac{\Omega_{\gamma0}H_0^2}{a^4H(a)^2} \quad \text{(Photon)} \tag{5}$$

$$\Omega_\nu(a) = \frac{\Omega_{\nu0}H_0^2}{a^4H(a)^2} \quad \text{(Neutrino)} \tag{6}$$

$$\Omega_\Lambda(a) = \frac{\Omega_{\Lambda0}H_0^2}{H(a)^2} \quad \text{(Dark Energy)} \tag{7}$$

which all are functions of the expansion coefficient $a(t)$ and should sum to 1. The density parameters $\Omega_{\gamma0}$ and $\Omega_{\nu0}$ are given as

$$\Omega_{\gamma0} = 2\cdot\frac{\pi^2}{30}\frac{(k_bT_{\text{CMB0}})^4}{\hbar^3c^5}\cdot\frac{8\pi G}{3H_0^2}, \tag{8}$$

$$\Omega_{\nu0} = N_{\text{eff}}\cdot\frac{7}{8}\left(\frac{4}{11}\right)^{4/3}\Omega_{\gamma0}, \tag{9}$$

where T_{CMB0} and H_0 is the temperature of the CMB and the Hubble constant today, and N_{eff} is the effective number of massless neutrinos. In general, values with "0" in the subscript refers to values measured in recent time. Then our Hubble parameter H can be written as

$$H = H_0\sqrt{\Omega_{R0}a^{-4} + \Omega_{M0}a^{-3} + \Omega_{k0}a^{-2} + \Omega_{\Lambda0}}, \tag{10}$$

where $\Omega_{\text{R0}} \equiv \Omega_{\gamma0} + \Omega_{\nu0}$ and $\Omega_{M0} \equiv \Omega_{b0} + \Omega_{\text{CDM0}}$. The distance travelled by a light from the Big Bang (often called the horizon) in a static universe would be ct if the Universe was not expanding. However, the Universe do expand, thus we must account for the expansion. This is done by using the conformal time η, given as

$$\frac{d\eta}{dt} = \frac{c}{a} \tag{11}$$

or equivalently by the chain rule

$$\frac{d\eta}{dx} = \frac{c}{\mathcal{H}} \tag{12}$$

where we have defined the logged expansion factor $x \equiv \ln(a)$ and the conformal Hubble factor $\mathcal{H} \equiv aH = \dot{a}$. This gives $\eta(x)$ as

$$\eta(x) = \int_{-\infty}^{x}\frac{cdx}{\mathcal{H}(x)}. \tag{13}$$

The conformal time is simply the distance light may have travelled since the big bang, and is also often referred to as the horizon or conformal time. Since conformal time is strictly increasing with time, we can use this as a time parameter. If we write the metric in spherical coordinates we would get

$$ds^2 = -c^2dt^2 + a^2\left(\frac{dr^2}{1-kr^2} + r^2d\theta^2 + r^2\sin\theta^2d\phi^2\right). \tag{14}$$

For photons, $ds^2 = 0$, which further gives us

$$cdt = \frac{adr}{\sqrt{1-kr}} \implies \int_t^{t_{\text{today}}}\frac{cdt}{a} = \int_0^r\frac{dr'}{\sqrt{1-kr'}}. \tag{15}$$

The LHS of Eq.(15) is

$$\chi \equiv \eta_0 - \eta(x) \tag{16}$$

and is called the co-moving distance, while the RHS of Eq.(15) can be evaluated to

$$r = \begin{cases} \chi\cdot\frac{\sin\left(\sqrt{|\Omega_{k0}|}H_0\chi/c\right)}{\left(\sqrt{|\Omega_{k0}|}H_0\chi/c\right)} & \Omega_{k0} < 0 \\ \chi & \Omega_{k0} = 0 \\ \chi\cdot\frac{\sinh\left(\sqrt{|\Omega_{k0}|}H_0\chi/c\right)}{\left(\sqrt{|\Omega_{k0}|}H_0\chi/c\right)} & \Omega_{k0} > 0 \end{cases}. \tag{17}$$

We would also like to compute the standard measures in cosmology. If we observe an object with the physical size D and angular size θ, we can define the angular distance d_A as

$$d_A \equiv \frac{D}{\theta}.$$

From the metric in Eq.(14), we can see that $dD = ard\theta$, giving

$$d_A = ar = re^x. \tag{18}$$

Next we want to know the luminosity distance d_L, which is defined as the distance to the light source. This can be found by the flux F of the source, given as

$$F = \frac{L}{4\pi d_L^2}$$

which gives

$$d_L = \frac{r}{a} = re^{-x} \tag{19}$$

Lastly, we want to compute the relation between the comic time t and the time-coordinate $x \equiv \ln(a)$. From

$$H = \frac{1}{a}\frac{d}{dt}a \Rightarrow dt = \frac{da}{aH}$$

we can finally find

$$t(x) = \int_0^a\frac{da}{aH} = \int_{-\infty}^x\frac{dx}{H(x)} \tag{20}$$

or as a differential

$$\frac{dt}{dx} = \frac{1}{H(x)}. \tag{21}$$

The last thing we will define here is the redshift z, which is given as

$$z = \frac{a_0}{a(t)} - 1 \tag{22}$$

1.1.2. MCMC-fits - Bayesian inference

Now, we will talk a little bit about MCMC-fitting. Consider some model parameters θ given some data X. What we really want to know, is the probability of our model given the data from the supernova, written as $P(\theta \,|\, X)$. What we will do is iteratively generate new parameters θ_{new}, and check if they fit the data better compared to our old parameters. To do this, we can use the well known Bayes theorem

$$P(\theta \,|\, X) = \frac{P(X \,|\, \theta)P(\theta)}{P(X)} \tag{23}$$

which relates

- $P(\theta \,|\, X)$: Probability of the model given the data (called posterior probability).
- $P(X \,|\, \theta)$: Probability of the data given the model (called likelihood).
- $P(\theta)$: The probability of our model (called prior probability).
- $P(X)$: The probability of the data (called evidence).

In order to fully calcualte the posterior, we will need the prior $P(\theta)$ and the likelihood $P(X \,|\, \theta)$ (it will become clear why the evidence $P(X)$ is not needed later). Given that we can get samples from the prior/likelihood, we can generate a new set of model parameters $\theta_{\text{new}} = \theta + N(0,1) \cdot \Delta\theta$, where $N(0,1)$ is a normal distribution with $\mu = 0$, $\sigma^2 = 1$ and $\Delta\theta$ is some stepsize. This is just a convenient way to ensure that you can step in both positive and negative directions, while keeping the stepsize small (as we don't want to make huge jumps in the parameter space).
Under the assumption that the likelihood for each data point $X_i \in X$ is a Gaussian, i.e. $P(X_i \,|\, \theta) \propto N(x_i(\theta), \sigma_i^2)$, and that each X_i is uncorrelated, we can recover the full likelihood as

$$P(X \,|\, \theta) = \prod_i P(X_i \,|\, \theta) \propto \exp\left[-\frac{1}{2}\sum_i \frac{(x_i(\theta) - X_i)^2}{\sigma_i^2}\right], \tag{24}$$

where $x_i(\theta)$ is the corresponding quantity to X_i given by the model and model-parameters θ. We can recognize the exponential as the χ^2, defined as

$$\chi^2 = \sum_{i=1}^{N} \frac{(x_i(\theta) - X_i)^2}{\sigma_i^2}. \tag{25}$$

Thus the likelihood is given as $P(X \,|\, \theta) \propto \exp\left[-\chi^2/2\right]$. By calculating χ^2, χ^2_{new} for the parameters θ, θ_{new}, we can now determine how likely the parameters are. If $\chi^2_{\text{new}} < \chi^2$, we immediately want to accept θ_{new} (store the value) and update $\theta = \theta_{\text{new}}$, as the new parameters are more likely. Then we can generate a new set of proposed parameters, and repeat.
If $\chi^2_{\text{new}} > \chi^2$, one could naively think that we would reject the parameters right away. This is not desirable as this would make us only accept samples giving the most likely parameters, meaning that we won't recover the full posterior $P(\theta \,|\, X)$ as we get stuck in a small region in parameter-space. What we really want to do is to still give it a chance to be accepted, given by the ratio

$$p = \frac{P(\theta_{\text{new}} \,|\, X)}{P(\theta \,|\, X)} = \exp\left[-\frac{1}{2}(\chi^2_{\text{new}} - \chi^2)\right].$$

If $p > u \in U(0,1)$, we accept θ_{new} and update $\theta = \theta_{\text{new}}$. If $p < u \in U(0,1)$, we reject θ_{new} and keep $\theta = \theta$. This is somehow the magic of MCMC. Notice that we never needed to know the evidence $P(X)$, nor the proportionality of $P(X \,|\, \theta)$, as they both cancel out in the ratio above.

A key-observation from Eq.(25) is that if the difference $x_i(\theta) - X_i \sim \sigma_i$, we will have that $\chi^2 \sim N$, or $\chi^2/N \sim 1$. This signifies a good fit, as the data has an intrinsic uncertainty (which we can not magically fit away). That is why $\chi^2 \ll N$ often is called "over-fitting", as $x_i(\theta) - X_i \sim 0$ does not necessarily mean that you have a good fit, since the data X_i has some uncertainty we can not get rid of by fitting. We can also have $\chi^2 \gg N$ which is called "under-fitting". Both under-fitting and over-fitting signifies bad fits.

1.2. Implementation, numerical methods and tests

From hereon, we will use the following values of parameters from Planck 2018 data [1] for calculations:

$$H_0 = 67\frac{\text{km/s}}{\text{Mpc}}, \tag{26}$$

$$T_{\text{CMB0}} = 2.7255\,K, \tag{27}$$

$$N_{\text{eff}} = 3.046, \tag{28}$$

$$\Omega_{\text{b0}} = 0.05, \tag{29}$$

$$\Omega_{\text{CDM0}} = 0.267, \tag{30}$$

$$\Omega_{k0} = 0. \tag{31}$$

Using Eq.(8) and Eq.(9) we can calculate $\Omega_{\gamma 0}$ and $\Omega_{\nu 0}$, and then using Eq.(1) we can find $\Omega_{\Lambda 0}$ as

$$\Omega_{\Lambda 0} = 1 - (\Omega_{k0} + \Omega_{b0} + \Omega_{\text{CDM0}} + \Omega_{\gamma 0} + \Omega_{\nu 0}). \quad (32)$$

Then using the parameterization $x = \ln(a)$ and Eq.(10) we find

$$H = H_0\sqrt{\Omega_{R0}e^{-4x} + \Omega_{M0}e^{-3x} + \Omega_{k0}e^{-2x} + \Omega_{\Lambda 0}}. \quad (33)$$

With the parameterization $x = \ln(a)$, the conformal Hubble factor $\mathcal{H}$ defined under Eq.(12) is now written $\mathcal{H} \equiv aH = e^x H$. Then we have

$$\mathcal{H} = H_0\sqrt{\Omega_{R0}e^{-2x} + \Omega_{M0}e^{-x} + \Omega_{\Lambda 0}e^{2x} + \Omega_{k0}}. \quad (34)$$

With all these at hand, we can solve the ODE's for the conformal time $\eta(x)$ and cosmic time $t(x)$. Both $H(x)$ and $\mathcal{H}(x)$ will be implemented as functions of x in the program.

1.2.1. *Solving the ODE's*

We start by solving the ODE's for conformal time $\eta(x)$ and cosmic time $t(x)$ given in Eq.(12) and Eq.(21). Numerically, this is done by an ODE-solver, and we choose to solve using the Runge-Kutta 4 algorithm (RK4). Instead of implementing the algorithm ourselves, we resort to using Gnu Scientific Library (GSL) and using the tools there.

1.2.2. *Splining*

After solving the ODE's we spline our result, meaning that we interpolate our numerical solution to points that we did not solve for, but still want to have. For example, say that I solve an ODE using RK4. I get a solution for $x = -0.1$ and $x = 0.1$, but I want to know the solution in $x = 0$. Then I can use spline to interpolate between $x = -0.1$ and $x = 0.1$ to get a value for $x = 0$. Again, we use the tools in GSL to make splines of the solutions.

Since we solve the ODE's for $\eta(x)$ and $t(x)$, we also spline both of these using a cubic spline. Spline also have methods for getting the derivatives, and we use those to get the first order derivatives of $\eta(x)$ and $t(x)$ wrt. x as well. We implement all these as functions.

1.2.3. *Calculated quantities*

We calculate the quantities $\Omega_k, \Omega_{\text{CDM}}, \Omega_b, \Omega_\gamma, \Omega_\nu, \Omega_\Lambda$ by using Eqs.(2),(3),(4),(5),(6),(7). We implement these as functions of x in the program by calling $H(x)$.

We would also like to find the luminosity distance d_L given in Eq.(19) and angular distance d_A given in Eq.(18), meaning that we must get r from Eq.(17) and χ from Eq.(16), using the solution of the ODE for $\eta(x)$. We implement $r(x)$ and $\chi(x)$ as functions, and use the splined result for $\eta(x)$.

We also calculate the first and second order derivatives of the conformal Hubble-factor $\mathcal{H}$. Sicne this is straight forward calculus, I will just state the results:

$$\frac{d\mathcal{H}}{dx} = \frac{H_0^2}{2H}\left(2\Omega_{\Lambda 0}e^x - 2\Omega_{R0}e^{-3x} - \Omega_{M0}e^{-2x}\right), \quad (35)$$

$$\begin{aligned}\frac{d^2\mathcal{H}}{dx^2} = &\frac{H_0^2}{2H}\left(2\Omega_{\Lambda 0}e^x + 6\Omega_{R0}e^{-3x} + 2\Omega_{M0}e^{-2x}\right) \\ &+ \frac{H_0^4}{4H^3}\left(4\Omega_{R0}e^{-4x} + 3\Omega_{M0}e^{-3x} + 2\Omega_{k0}e^{-2x}\right) \\ &\left(2\Omega_{\Lambda 0}e^x - 2\Omega_{R0}e^{-3x} - \Omega_{M0}e^{-2x}\right).\end{aligned} \quad (36)$$

We would also like to find an expression for $\frac{d^2a}{dt^2} = \ddot{a}$ so that we can find when $\ddot{a} \geq 0$, as this will tell us when the Universe starts accelerating. Since we have $\mathcal{H} = \dot{a}$, we can use the chain-rule to obtain

$$\ddot{a} = \frac{d\dot{a}}{dt} = \frac{d\mathcal{H}}{dt} = \frac{d\mathcal{H}}{dx}\frac{dx}{dt}.$$

Now, since $x = \ln a$, we get

$$\frac{dx}{dt} = \frac{\dot{a}}{a} = \mathcal{H}e^{-x},$$

giving

$$\ddot{a} = \mathcal{H}\frac{d\mathcal{H}}{dx}e^{-x} \quad (37)$$

in terms of quantities we have from Eq.(35) and Eq.(34).

1.2.4. *MCMC-fits - Bayesian inference*

We will use a Markov Chain Monte Carlo sampler (MCMC-sampler) to sample values for the parameters $\theta = (h, \Omega_M, \Omega_k)$ with a given data set D from [2] (supernova data). Essentially, we will use Ω_k to find Ω_Λ by $\Omega_\Lambda = 1 - (\Omega_M + \Omega_k)$, and $h \propto H_0$.

The evidence $P(D)$ in Eq.(23) is usually very difficult to find, but we won't need to know this as it cancels in the algorithm, as shown in Sec.(1 1.1).
In order for us to calculate the posterior, we need to have prior knowledge about our model. This is essentially what leads us to the choice of parameters $\theta = (h, \Omega_M, \Omega_k)$, as we know $\Omega_M \in [0, 1]$ and $\Omega_k \in [-1, 1]$ (as for h, we seemingly just make a choice). Thus we use uniform distributions as priors, meaning that

$$\begin{aligned}P(h) &= U(0.5, 1.5), \\ P(\Omega_M) &= U(0, 1), \\ P(\Omega_k) &= U(-1, 1).\end{aligned}$$

Next, we would want to find out if the proposed parameters θ_{new} are good or not, and this is where the supernova data comes in. We denote the luminosity distance from the supernova data for a given redshift z_i as $D_i = d_L^{\text{obs}}(z_i) \in D$, and from our model as $d_i = d_L(z_i, \theta)$. Given the same assumptions leading to Eq.(24), we have a likelihood $P(D\,|\,\theta) \propto \exp\left[-\chi^2/2\right]$ with

$$\chi^2 = \sum_{i=1}^{N} \frac{(d_i(\theta) - D_i)^2}{\sigma_i^2}$$

from Eq.(25). Thus the only remaining step is to run the algortihm described in Sec.(1 1.1).

1.2.5. Testing

To test what we have implemented we can make some simple approximations, and check if the approximation matches the implementation. We will now do this for $\mathcal{H}$ using Eq.(34).
In the X-dominated era, we expect that the density-parameter $\Omega_X \approx 1$, and have the remaining $\Omega_i \approx 0$. I denote the dominaiton-era by a subscript, giving the approximations $\mathcal{H}_X$ of the conformal Hubble-factor by

$$\begin{aligned}
\mathcal{H}_R &= H_0\sqrt{\Omega_{R0}}e^{-x}, \\
\mathcal{H}_M &= H_0\sqrt{\Omega_{M0}}e^{-\frac{1}{2}x}, \\
\mathcal{H}_\Lambda &= H_0\sqrt{\Omega_{\Lambda 0}}e^{x},
\end{aligned} \tag{38}$$

which gives the simple expressions for the derivatives

$$\begin{aligned}
\frac{1}{\mathcal{H}_R}\frac{d\mathcal{H}_R}{dx} &= -1, & \frac{1}{\mathcal{H}_R}\frac{d^2\mathcal{H}_R}{dx^2} &= 1, \\
\frac{1}{\mathcal{H}_M}\frac{d\mathcal{H}_M}{dx} &= -\frac{1}{2}, & \frac{1}{\mathcal{H}_M}\frac{d^2\mathcal{H}_M}{dx^2} &= \frac{1}{4}, \\
\frac{1}{\mathcal{H}_\Lambda}\frac{d\mathcal{H}_\Lambda}{dx} &= 1, & \frac{1}{\mathcal{H}_\Lambda}\frac{d^2\mathcal{H}_\Lambda}{dx^2} &= 1.
\end{aligned} \tag{39}$$

Then by Eq.(13) we can find approximations $\eta_X(x)$

$$\begin{aligned}
\eta_R &= \frac{c}{H_0\sqrt{\Omega_{R0}}}e^{x}, \\
\eta_M &= \eta_R(x_M) + \frac{2c}{H_0\sqrt{\Omega_{M0}}}\left(e^{\frac{1}{2}x} - e^{\frac{1}{2}x_M}\right), \\
\eta_\Lambda &= \eta_M(x_\Lambda) - \frac{c}{H_0\sqrt{\Omega_{\Lambda 0}}}\left(e^{-x} - e^{-x_\Lambda}\right),
\end{aligned} \tag{40}$$

where x_M and x_Λ is the x-values where matter and dark energy-domination begins respectively. Numerically I choose this to be at radiation-matter equality and matter-dark energy equality to simplify, since we will find these values anyway. We make the plots, and the result of the test can be seen in Fig.(1) and Fig.(2)

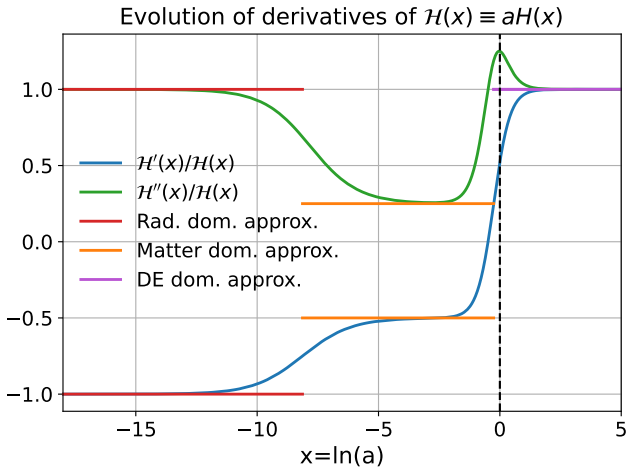

FIG. 1: Plot of the first and second order derivatives of the conformal Hubble factor $\mathcal{H}$ divided by $\mathcal{H}$ (blue and green). The straight lines are analytical approximations to the different domination eras.

In Fig.(1) we can see a plot of the first and second order derivatives of the conformal Hubble factor $\mathcal{H}$ wrt. x, divided by $\mathcal{H}$. The straight lines in Fig.(1) are approximations given in Eq.(39) in the different domination eras, which we can see lies tangent to the numerically computed graphs, which is a good sign. We can also see how the approximations quickly goes wrong in the matter-dominated and Dark energy-dominated era.

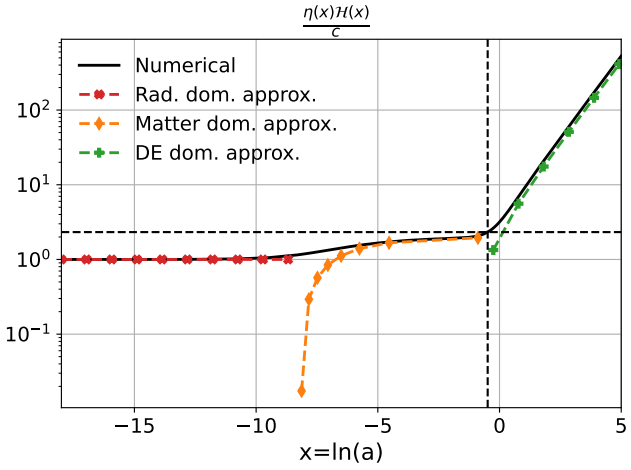

FIG. 2: Plot of $\frac{\eta(x)\mathcal{H}(x)}{c}$ compared to analytical approximations in different domination eras. The cross indicates when acceleration of the Universe happens in x and the value of $\frac{\eta(x)\mathcal{H}(x)}{c}$. The markers are added only for visibility, the approximations are analytical.

We also have a similar to the one in Fig.(1) for $\frac{\eta(x)\mathcal{H}(x)}{c}$, which can be seen in Fig.(2). Again, the colored lines refer to analytical approximations in different domination

eras, where we just multiplied the approximations from Eq.(38) and Eq.(40). It is also clear that the approximation quickly goes wrong when we don't have dominated eras. Where we have different domination-eras can be more clearly seen in Fig.(6)

1.3. Results and discussion

Now that we done a couple of tests on the data to show that it gives promising results in the dominated regions, we can go on to look at some results.

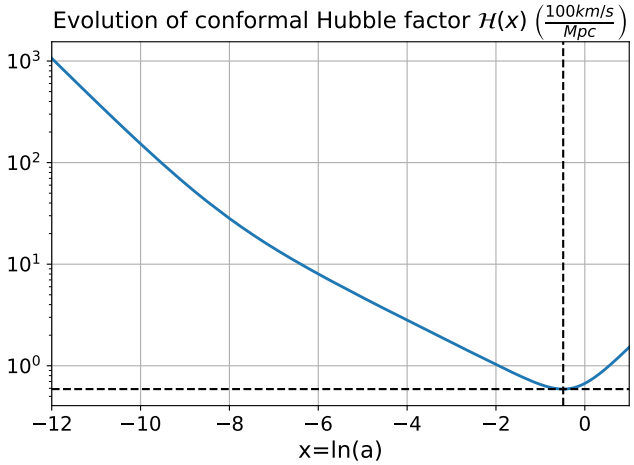

FIG. 3: Plot of the evolution of the conformal Hubble factor $\mathcal{H}$. The cross indicates when acceleration of the Universe happens in x and the value of $\mathcal{H}$.

In Fig.(3) we have plotted the evolution of the conformal Hubble factor $\mathcal{H}$. What is interesting in Fig.(3) is the turning-point, which coincides with the acceleration of the Universe.

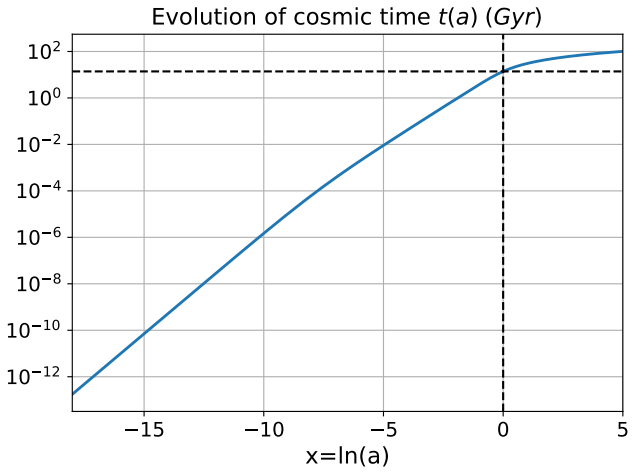

FIG. 4: Plot of the evolution of the cosmic time $t(x)$. The cross indicates the value of x and $t(x)$ today.

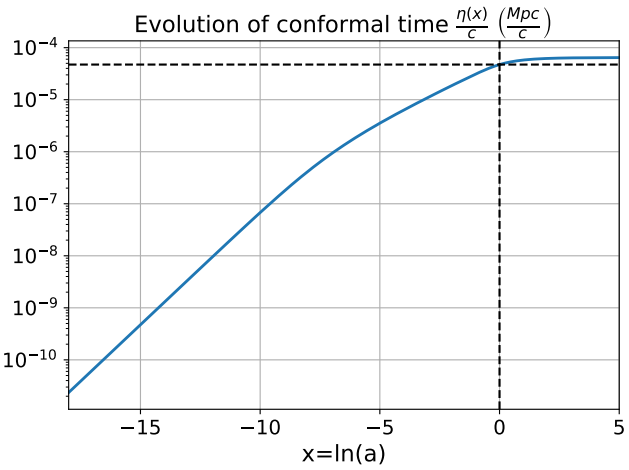

FIG. 5: Plot of the evolution of the conformal time $\eta(x)/c$. The cross indicates the value of x and $\eta(x)/c$ today.

In Fig.(4) and Fig.(5) we marked the values for $x = 0$, meaning the values of today, since these would be the most interesting. Both conformal and cosmic time is monotonically increasing, which is a good sign since they represent time.

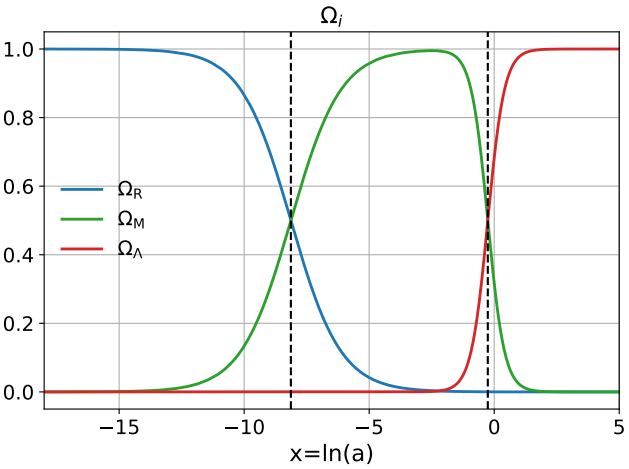

FIG. 6: Plot of the evolution of density parameters $\Omega_R = \Omega_\gamma + \Omega_\nu$, $\Omega_M = \Omega_b + \Omega_{\text{CDM}}$ and Ω_Λ. The dashed lines indicate Radiation-Matter equality and Matter-Dark Energy equality.

In Fig.(6) we can see the evolution of the density parameters $\Omega_R = \Omega_\gamma + \Omega_\nu$, $\Omega_M = \Omega_b + \Omega_{\text{CDM}}$ and Ω_Λ. The dashed lines indicate domination-era equalities, where the dominating regime change. An interesting consequence of Eq.(37) from this is that we get acceleration when $\Omega_\Lambda \geq \frac{1}{3}$. This can be shown by using Eq.(35) in the regime where $\Omega_R \approx 0$. Using the definitions given in

Eq.(3), Eq.(4) and Eq.(7) we can write

$$\frac{d\mathcal{H}}{dx} = \frac{H_0^2}{2H}\left(2\Omega_{\Lambda 0}e^{x} - 2\Omega_{R0}e^{-3x} - \Omega_{M0}e^{-2x}\right)$$
$$\approx He^{x}\left(\Omega_\Lambda - \frac{1}{2}\Omega_M\right).$$

Then, using $\mathcal{H} = He^x$ Eq.(37) becomes

$$\ddot{a} = \mathcal{H}\frac{d\mathcal{H}}{e^x} \approx H^2 e^x\left[\Omega_\Lambda - \frac{1}{2}\Omega_M\right].$$

Acceleration of the Universe happens when $\ddot{a} \geq 0$. Since $H^2 \geq 0$ and $e^x \geq 0$, we only need

$$\Omega_\Lambda - \frac{1}{2}\Omega_M \geq 0.$$

Since in this era, $\Omega_R \approx 0$, we have $\Omega_\Lambda + \Omega_M = 1$. Thus we get

$$\Omega_\Lambda - \frac{1}{2}\Omega_M = \frac{3}{2}\Omega_\Lambda - \frac{1}{2} \geq 0 \Rightarrow \Omega_\Lambda \geq \frac{1}{3}.$$

This means that the Universe starts to accelerate when $\Omega_\Lambda \approx \frac{1}{3}$. Numerically, we find this value to be $\Omega_\Lambda = 0.333489$ when the Universe accelerated, which coincides with the predicted value of $\Omega_\Lambda \approx \frac{1}{3}$ from the theory.

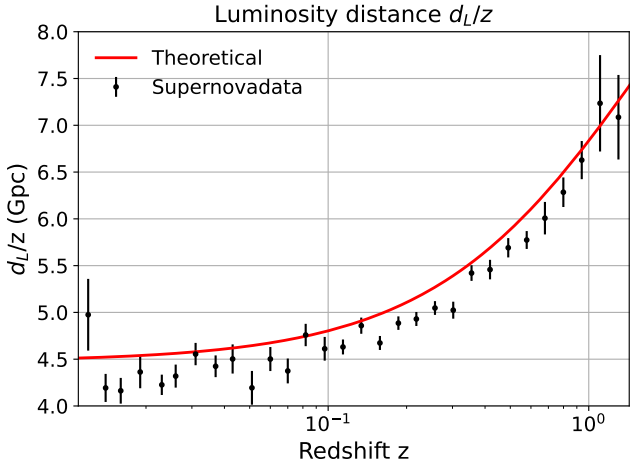

FIG. 7: Plot of the luminosity distance d_L pr. redshift z. We plot both the theoretical prediction and measured data with errorbars.

In Fig.(7) we can see a plot of the luminosity distance d_L plotted for both theoretical model and numerical data from the supernova data in [2]. However, in Fig.(7) we can see that our model consistently lies slightly above the recorded data.

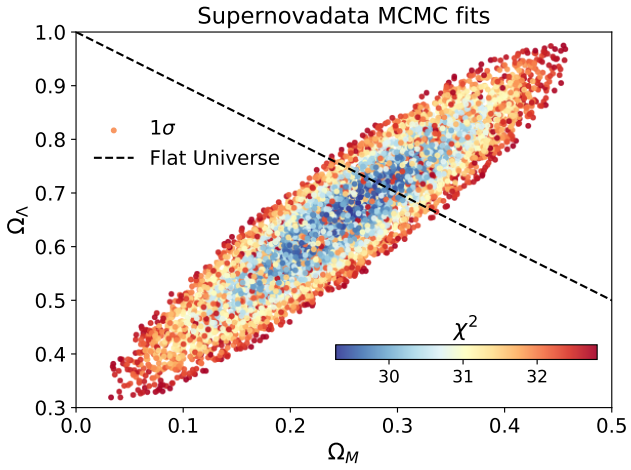

FIG. 8: Scatter plot of the MCMC fits of the supernova data in 1σ constraint. The straight line refers to a flat universe, i.e. $\Omega_\Lambda + \Omega_M = 1$.

In Fig.(8) we can see a scatter plot from the MCMC fits of the supdernova data from [2] within the constraint of 1σ. According to Fig.(8) there is seemingly many combinations of Ω_Λ and Ω_M that would fit the supernova data within the given constraints. However, the inclusion of a flat Universe heavily reduces the number of possible combinations, as only data points crossing the dashed line in Fig.(8) would be of relevance.
Another important thing that Fig.(8) tells us is the content of the universe. By reading off, we can se that within a 1σ interval that Ω_M ranges between $\sim 0.03 - 0.45$ and Ω_Λ ranges between $\sim 0.31 - 0.97$. Adding the constraint of a flat Universe, we would find that Ω_M ranges between $\sim 0.23 - 0.33$ and Ω_Λ ranges between $\sim 0.66 - 0.76$. This tells us that the Universe should be somewhere in between $23 - 33\%$ matter, and $66 - 76\%$ dark energy. Thus we should also expect the cosmological constant Λ to be non-zero, meaning that we are forced to have dark energy in our Universe.

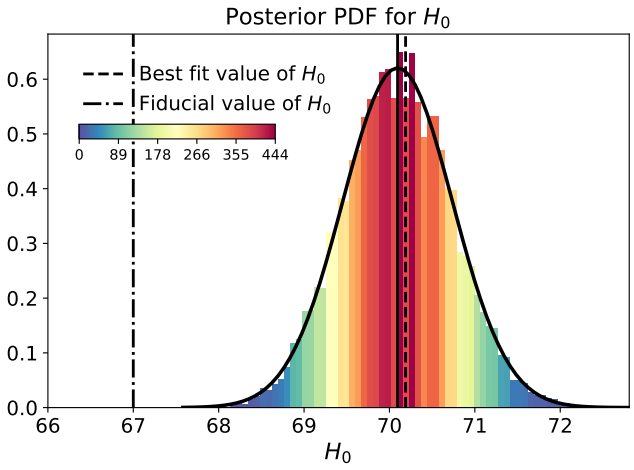

FIG. 9: Posterior PDF (Probability distribution function) of the Hubble Parameter today H_0. The colorbar indicates how many counts where considered in the bin, and the thick black line is a gaussian. The best fitted value of H_0 is close to the mean μ, while the fiducial value H_0 is the one we used.

Finally, in Fig.(9) we can see the posterior PDF of the Hubble parameter today, H_0, given from the MCMC fits. According to Fig.(9) it seems like the PDF follows a gaussian distribution. The mean of the distribution is marked with a solid black vertical line, and has the value of $\mu = 70.095\text{s}^{-1}$. The dashed black vertical line signifies the best fitted value of H_0 from the MCMC fits, with the value $H_0^{\text{best fit}} = 70.189\text{s}^{-1}$ and $\chi^2 = 29.281$ (or since $N = 31$ we have $\chi^2/N = 0.945$), signaling a good fit ($\chi^2/N \sim 1$ means good). The value for $H_0^{\text{best fit}}$ is slightly off with the mean μ as seen in Fig.(9). However, very noticeably in Fig.(9) we can see that our value for H_0 lies far off from the sampled values of H_0, even further away than 3σ. This is called "the Hubble tension problem", but this won't be discussed any further.

TABLE I: Table that contains values for important events.

Event	x	z	t (Gyr)
Rad.-Matter equality	-8.132	3400.530	$5.106 \cdot 10^{-5}$
Matter-DE equality	-0.256	0.291	10.379
Universe accelerate	-0.486	0.627	7.757
Today	0.000	0.000	13.857

In Tab.(I) one can see values of x, z and t in important and relevant events. One of the most interesting results would be the cosmic time Today, $t(0)$, which we see in Tab.(I) is found as $t_{\text{today}} = 13.857\,\text{Gyr}$. According to [1], the age of the universe is estimated to be $t_{\text{today}} = 13.830 \pm 0.037\,\text{Gyr}$, meaning that our result is within the measurements from Planck 2018.

1.4. Conclusions

We solved the ODE's for conformal time η/c and cosmic time t. We also derived the Hubble factor H, and related these quantities to other relevant cosmological factors. Then we performed a MCMC fit to data from a supernova, to give us the best fitted values for H_0, Ω_M and Ω_k.
From the MCMC-fitting of the supernovadata we found that in a flat Universe, we are forced to have Dark Energy an matter in our Universe, with an abundance of $\sim 66 - 76\%$ and $\sim 23 - 33\%$, respectively.
We also predicted an acceleration of the Universe around $\Omega_\Lambda \approx \frac{1}{3}$, which we numerically found to be $\Omega_\Lambda \approx 0.333489$. This happened at time $t = 7.577\,\text{Gyr}$. Further, we discovered the age of the Universe the be $t \approx 13.857\,\text{Gyr}$.
In final conclusion, the data predicted from the model seems to correspond well with observational data. Thus we have good reason to believe that we so far have a correct implementation of the model.

2. MILESTONE II

In this Milestone, our goal would be to investigate the recombination of the Universe. Recombination is usually referred to as the time when the Universe got optically thin, or the photons from the CMB decoupled from thermal equilibrium of the early Universe. The event of decoupling photons is also often called *last scattering*, and these are the photons we observe today. Recombination occurs due to the expansion of the Universe, causing the photons to become less energetic - cooling down the Universe. This means less energetic photons will be emitted, and electrons will no longer be ionized from atoms. Since the binding energy of hydrogen is 13.6 eV, one might naively think that this is the energy requirement for the photons. However, when the mean energy of the photons reach ~ 0.25eV, the free electrons previously ionized can now form neutral hydrogen with free protons. At some point, the photons will scatter with free electrons for the last time, as a sufficient amount of electrons and protons have formed neutral matter.
In this Milestone, we will calculate the optical depth $\tau(x)$ in Eq.(41), and the visibility function $\tilde{g}(x)$ in Eq.(12) which we will need in later Milestones. We will also consider the sound horizon $s(x)$ in Eq.(50), which will be of great importance in later Milestones.

2.1. Theory

2.1.1. Saha- and Peebles equation

In the early times, the Universe was a tightly coupled plasma of protons and electrons. The photons from the CMB tried to travel through this medium, but due to the dense plasma it was absorbed. If we have a light-source at $x = 0$ with intensity I_0, an observer at position r will obeserve an intensity

$$I(r) = I_0 \exp[-\tau(r)],$$

where $\tau(r)$ is the optical depth. The optical depth is defined as

$$\tau(\eta) = \int_{\eta}^{\eta_0} n_e \sigma_T a d\eta',$$

or more conveniently for this section written in our time-parameter x

$$\tau(x) = -\int_{x_0}^{x} \frac{c n_e \sigma_T}{H}\, dx' \rightarrow \frac{d\tau(x)}{dx} = -\frac{c n_e \sigma_T}{H}, \quad (41)$$

where $H(x)$ is the Hubble factor, σ_T is the Thompson-scattering cross section, and $n_e(x)$ is the electron number density. In Eq.(41) we only need to find n_e since everything else is known. Rather than computing n_e directly, we define the fractional electron density X_e as

$$X_e = \frac{n_e}{n_H}, \quad (42)$$

where n_H is the hydrogen density given as

$$n_H = (1 - Y_p) n_b = (1 - Y_p) \frac{\Omega_{b0} \rho_{c0}}{m_H a^3}. \quad (43)$$

In Eq.(43) n_b is the baryon density, m_H is the hydrogen mass, ρ_{c0} is the critical density today, and Y_p is the Helium fraction. We will assume that $Y_p = 0$.
From the Boltzmann-equation

$$\frac{df}{dt} = C[f] \quad (44)$$

where $f(\vec{r}, \vec{p}, t)$ is the probability density function of the phase-space, and $C[f]$ is some collision term for a given reaction. For a $e^- + p^+ \rightleftharpoons H + \gamma$ process, it can be derived from the Boltzmann-equation that

$$\frac{1}{a^3} \frac{d(n_e a^3)}{dt} = -(n_e n_p)_{\text{eq}} \langle \sigma v \rangle \left(\frac{n_e n_p}{(n_e n_p)_{\text{eq}}} - \frac{n_H n_\gamma}{(n_H n_\gamma)_{\text{eq}}} \right). \quad (45)$$

In the situation where the LHS $\ll$ RHS in Eq.(45), we must then have

$$\frac{n_e n_p}{(n_e n_p)_{\text{eq}}} = \frac{n_H n_\gamma}{(n_H n_\gamma)_{\text{eq}}}$$

to balance out the equation. Notice that this is $\approx$ and not $=$, as an equality would give 0 in Eq.(45). Even though it is an approximation, we write it with with $=$. Since the Universe is electrically neutral, we can use $n_e = n_p$. Also, since the photons still are in equilibrium with the primordial plasma at early times we have $n_\gamma = (n_\gamma)_{\text{eq}}$, and since we already assumed no helium ($Y_p = 0$, and other heavier elements) we have $n_b \approx \rho_b / m_H$. Combining all this gives another convenient equation for X_e,

$$\frac{X_e^2}{(1 - X_e)} = \frac{1}{n_b} \left(\frac{m_e k_b T_b}{2\pi\hbar^2} \right)^{3/2} \exp\left[-\frac{\epsilon_0}{k_b T_b} \right], \quad (46)$$

referred to as the Saha-equation. In Eq.(46) m_e is the electron mass, T_b is the baryon temperature, k_b is the Boltzmann constant, and $\epsilon_0 = 13.6\text{eV}$ is the ionization energy of hydrogen. However, the Saha-equation is just an approximation that works for $X_e \approx 1$. Since photons fall out of equilibrium with the priomordial plasma as soon neutral hydrogen starts to form, we need to consider a changing abundance in n_e. Whenever this is the case, we can not use Eq.(46). Thus we need another equation for X_e

$$\frac{dX_e}{dx} = \frac{C_r(T_b)}{H} \left[\beta(T_b)(1 - X_e) - n_H \alpha^{(2)}(T_b) X_e^2 \right], \quad (47)$$

known as the Peebles-equation, which is derived from the Boltzmann-equation in Eq.(45). A derivation of this equation can be found in [6], but it is really Eq.(45) with some additional advanced atomic physics. The terms in Eq.(47) are

$$\begin{aligned}
C_r(T_b) &= \frac{\Lambda_{2s\rightarrow 1s} + \Lambda_\alpha}{\Lambda_{2s\rightarrow 1s} + \Lambda_\alpha + \beta^{(2)}(T_b)}, && \text{(dim. less)} \\
\Lambda_{2s\rightarrow 1s} &= 8.227\text{s}^{-1}, && \text{(dim. 1/s)} \\
\Lambda_\alpha &= H \frac{(3\epsilon_0)^3}{(8\pi)^2 c^3 \hbar^3 n_{1s}}, && \text{(dim. 1/s)} \\
n_{1s} &= (1 - X_e) n_H, && \text{(dim. 1/m}^3\text{)} \\
n_H &= (1 - Y_p) n_b, && \text{(dim. 1/m}^3\text{)} \\
n_b &= (1 - Y_p) \frac{3 H_0^2 \Omega_{b0}}{8\pi G m_H a^3}, && \text{(dim. 1/m}^3\text{)} \\
\beta^{(2)}(T_b) &= \beta(T_b) e^{\frac{3\epsilon_0}{4 k_b T_b}}, && \text{(dim. 1/s)} \\
\beta(T_b) &= \alpha^{(2)}(T_b) \left(\frac{m_e k_b T_b}{2\pi\hbar^2} \right)^{3/2} e^{-\frac{\epsilon_0}{k_b T_b}}, && \text{(dim. 1/s)} \\
\alpha^{(2)}(T_b) &= \frac{8}{\sqrt{3\pi}} c \sigma_T \sqrt{\frac{\epsilon_0}{k_b T_b}} \phi_2(T_b), && \text{(dim. m}^3\text{/s)} \\
\phi_2(T_b) &= 0.448 \ln\left(\frac{\epsilon_0}{k_b T_b} \right). && \text{(dim. less)}
\end{aligned} \quad (48)$$

2.1.2. The visibility function

Finally we need to define the visibility function $\tilde{g}(x)$, given as

$$\tilde{g}(x) = -\tau'(x) \cdot e^{-\tau(x)} \tag{49}$$

with τ given in Eq.(41). An interesting property of $\tilde{g}(x)$ is

$$\int_{-\infty}^{0} \tilde{g}(x)dx = 1,$$

and $\tilde{g}(x)$ is therefore a probability density function (PDF). The visibility function describes the probability of a photon reaching us today last being scattered at time x. The last thing we will define in this section is the sound-horizon which is defined as

$$s(x) = \int_{-\infty}^{x} \frac{c_s dx}{\mathcal{H}} \to \frac{ds(x)}{dx} = \frac{c_s}{\mathcal{H}}, \tag{50}$$

where c_s is the sound-speed defined as

$$c_s = c\sqrt{\frac{R}{3(1+R)}}, \quad R = \frac{4\Omega_{\gamma 0}}{3\Omega_{b0}}e^{-x}.$$

Physically, the sound horizon represents the distance a sound-wave in the photon-baryon plasma can propagate from the Big Bang and until photons decouple from matter. This will be investigated further in Milestone 3.

2.2. Implementation, numerical methods and tests

We will assume $Y_p = 0$ in the calculations below.

2.2.1. Solving the Saha- and Peebles-equation

The reason we need both the Saha- and Peebles-equation for X_e (Eq.(46) and Eq.(47)) is because the Peebles-equation is numerically unstable in early times. Thus we need to solve the Saha-equation to get a stable solution. Solving the Saha-equation does not rely on any ODE-solving - it is simply a second order polynomial. Solving Eq.(46) for X_e yields

$$\frac{X_e^2}{(1-X_e)} = \frac{1}{n_b}\left(\frac{m_e k_b T_b}{2\pi\hbar^2}\right)^{3/2} \exp\left[-\frac{\epsilon_0}{k_b T_b}\right] = M,$$

$$\Rightarrow \quad X_e^2 + MX_e - M = 0,$$

which has solutions

$$X_e = \frac{M}{2}\left(-1 \pm \sqrt{1+\frac{4}{M}}\right).$$

Now, since we want X_e to be a positive number, and M is a positive number (only contains positive quantities), the correct solution is the one with + which finally gives

$$X_e = \frac{M}{2}\left(-1 + \sqrt{1+\frac{4}{M}}\right).$$

Notice that $M = M(x)$ as both $n_b(x)$ and $T_b(x)$ are functions of x. We have to be careful about the limits of $M \to 0$ and $M \to \infty$ (especially when doing numerics) - from the above equations we can see that M goes as

$$M \sim 10^{21} \cdot \frac{T_b^{3/2}}{n_b} \exp\left[\frac{\epsilon_0}{k_b T_b}\right].$$

We also have that

$$\frac{1}{n_b} \sim e^{3x}, \quad T_b \sim e^{-x},$$

so

$$M \sim 10^{21} \cdot e^{3x/2} e^{-10^4 \exp(x)}$$

For values $|x| \gg 1$, we can see that $M \to 0$. But for values around $10^4 \cdot \exp(x) \sim 1$ we have $x \sim -9$, which gives $M \sim 10^{14}$. Therefore we have to be careful when we are in the early universe. When M is very large, we can use the approximation

$$\sqrt{1+x} \approx 1 + \frac{x}{2}$$

to evalutate

$$\begin{aligned} X_e &= \frac{M}{2}\left(-1 + \sqrt{1+\frac{4}{M}}\right) \\ &\approx \frac{M}{2}\left(-1 + 1 + \frac{1}{2}\cdot\frac{4}{M}\right) \\ &= 1. \end{aligned}$$

We implement this by an if-test checking if $4/M < \varepsilon$ with a $\varepsilon = 10^{-7}$ as a tolerance, returning $X_e = 1$ if satisfied, and returning the original expression for X_e otherwise.

Since we later on would want to compare the Saha-solution to the combined Saha-Peebles-solution, we have to compute the Saha-equation in the limit where $M \to 0$. Then it is not hard to see that

$$\lim_{M\to 0} X_e = \lim_{M\to 0} -\frac{M}{2} + \frac{1}{2}\sqrt{M^2+4M} = 0,$$

meaning that values of X_e from the Saha-solution in this regime that becomes negative or nan, will just be replaced with 0. Since the Saha-equation only holds for $X_e \approx 1$, we will simply switch to solving the Peebles-equation Eq.(47) whenever $X_e < 0.99$. Solving the Peebles-equation is done by using the ODESolver from

the GSL-library, initializing using the last value from the Saha-solution and only solving on the remaining regime. Another thing we have to be careful about is the expression for $\beta^{(2)}$ in Eq.(48), as T_b might become very small making the exponential extremely big. This is solved simply by just inserting the expression for β into $\beta^{(2)}$, as adding the exponentials would make it well behaved.

After obtaining the solution for X_e we can easily use Eq.(42) to obtain the electron density n_e. We also might want to evaluate the solutions at points we did not solve for, so we also spline the solutions for X_e and n_e. However, since the solution of n_e varies over several orders of magnitude, we will instead spline $\ln(n_e)$, and exponentiate it later.

2.2.2. Calculating optical depth and visibility function

With the solution of $n_e(x)$, we can solve for the optical depth $\tau(x)$. This is done directly by using Eq.(41). However, we want to ensure that the optical depth today ($x_0 = 0$) is $\tau(x = x_0) = 0$. Thus our initial condition for the ODE is really our final (end time) condition. We could choose arbitrary initial values, and subtract $\tau(0)$ from $\tau(x)$ to get correct $\tau(x)$. However, this may lead to truncation-errors. Therefore, we choose to integrate backwards in time instead, as a more elegant solution. This is implemented by considering

$$\tau(x) = \int_x^{x_0} f(x)dx$$

with $x_0 > x$. Since our initial condition is for x_0, we need to flip the integration bounds. This gives

$$\tau(x) = -\int_{x_0}^{x} f(x)dx.$$

Thus by making an array (linspace) from x_0 to x, and implementing the RHS of the ODE in Eq.(41) as

$$f(x) = \frac{\sigma_T c n_e(x)}{H(x)}$$

we integrate backwards with negative dx. Lastly, we have to reverse the solution for $\tau(x)$ and the array x to get in in correct order.

To calculate the visibility-function $\tilde{g}(x)$ we then use Eq.(49) and the solution for the optical depth $\tau(x)$ and $\tau'(x)$ that we got from solving Eq.(41). Finally, we spline the results. To get the derivatives, we explicitly make arrays and use expressions for the first order derivatives τ' and $\tilde{g}'$ and spline them. The second order we get from calling the $.deriv\_x(x)$-method in Spline.

2.3. Results and discussion

In Fig.(10) we can see a plot of the fractional electron density X_e. The blue line is the combined Peebles-Saha solution, while the green dashed line is a pure Saha solution. It is clear from Fig.(10) that the Saha-solution tends to zero rather quickly, while the combined solution decreases more slowly and approaches some constant value which is represented as the purple dot-dashed line. The decrease in X_e is due to free electrons and free protons forming neutral hydrogen, making the Universe less optically thick. The constant value is the abundance of free electrons today, found to be $X_e(x = 0) = 2.02 \cdot 10^{-4}$. This makes sense, as it after some time becomes highly unlikely for free electrons to combine due to the reduced density. The density also reduces due to expansion of the Universe, making the distance between the baryons larger.

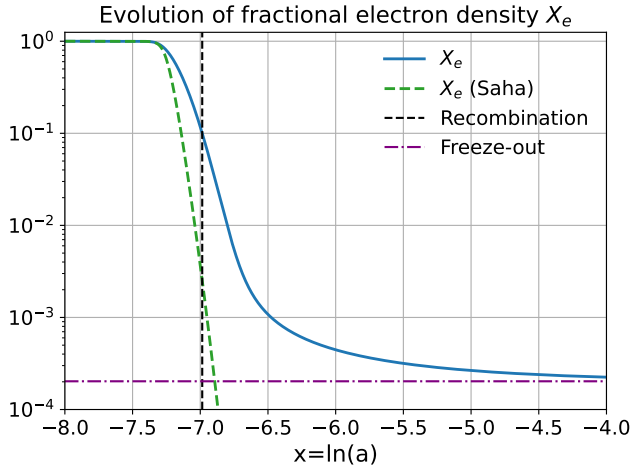

FIG. 10: Evolution of fractional electron density X_e solved with pure Saha-equation and the Saha-Peebles combination. $X_e = 0.1$ is pr. definition when recombination happens.

Fig.(11) shows the optical depth $\tau(x)$ and its two first derivatives. The black dashed line represents the time of last scattering. In Fig.(11), last scattering is occurring at $\tau = 0.97$, while the Universe transition between optically thick and optically thin at $\tau = 1$ (pr. definition). The same decrease seen in Fig.(10) for X_e can be seen in Fig.(11) for $\tau(x)$, occurring at the same time. The decrease happens over a magnitude $\sim 10^4$ as seen in Fig.(11), making the Universe transition from optically thick to optically thin. This ultimately allows photons from the CMB to travel without interacting with any free electrons, which is what we call recombination.

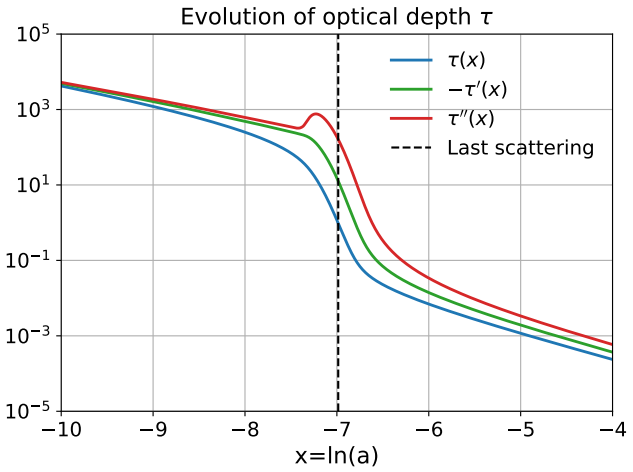

FIG. 11: Evolution of optical depth $\tau(x)$ and its derivatives. The dashed line represents the time of last scattering.

The visibility function $\tilde{g}(x)$ and its two first derivatives can be seen in Fig.(12). As stated in the theory section, the visibility function is a PDF, meaning that it is interpreted as a probability density. The visibility function describes the probability of a photon reaching us today last being scattered at time x, meaning that the most probable time the photons we observe last being scattered is at its peak $\tilde{g}_{\max}$. Therefore, this serves a good definition for when last scattering happened, which we have used. This can be seen in Fig.(12), as the dashed line perfectly aligns with the peak of $\tilde{g}$.

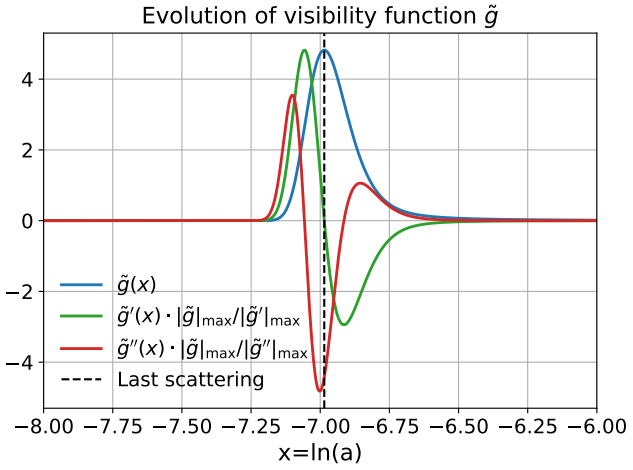

FIG. 12: Evolution of the visibility-function $\tilde{g}(x)$ and its derivatives, re-scaled appropriately. $\tilde{g}(x)$ is not re-scaled, so we can still interpret it as an PDF. The derivatives is scaled with $|\tilde{g}_{\max}|/|\tilde{g}'|_{\max} = 0.09712 \approx 1/10$ and $|\tilde{g}_{\max}|/|\tilde{g}''|_{\max} = 0.00502 \approx 1/200$.

From Fig.(10) and Fig.(11), we can then see that recombination did not happen instantaneously, but on a relatively short period in which neutral hydrogen was produced rapidly. On approximately the same time interval, we can also see that the visibility function in Fig.(12) sharply peaks, meaning that the last scattering most probably happened some time during the recombination. This is consistent with Fig.(10) since the amount of free electrons in early times is so large that it is very unlikely that it would be the last time the photon scattered, and in later times where the amount of free electrons is so low that it is unlikely that the photons will scatter at all.

An additional observation is that the optical depth τ in Fig(11) follows the same shape as the fractional electron density X_e in Fig.(10), but slightly tilted in a downwards direction. This is because the Universe is expanding, which can be seen in the optical depth in Fig.(11) as the tilt in the curve. The expansion of the Universe contributes to decreasing the optical depth by increasing the distance between matter, ultimately allowing photons to travel more freely. It also becomes clear that the production of neutral hydrogen in recombination happens at a faster rate than the expansion of the Universe.

TABLE II: Table that contains values for important events.

Event	x	z	t (Myr)	r_s (Mpc)
Recombination	-6.98551	1079.86	0.37793	145.290
Last scatter	-6.98539	1079.73	0.37801	145.302

In Tab.(II) we have the values of x, z, t, and r_s (sound horizon) in both recombination and last scattering. We can see that last scattering happened shortly after recombination. We can also see that the redshift for both events are $z \approx 1100$. We also got a sound horizon at $r_s = 145.302$Mpc and $r_s = 145.290$Mpc for last scattering and recombination. According to [1], they have a meaured value of $r_s = 144.46 \pm 0.48$Mpc, so compared to this our result is a bit off.

2.4. Conclusions

From our discussion above we can conclude that recombination did not happen instantaneously, but over a relatively short period in time at a much faster rate than the expansion of the Universe. The fractional electron density rapidly decreased over several orders of magnitude due to free electrons and protons forming neutral hydrogen, which together with the expansion of the Universe made the Universe transition from optically thick to optically thin (as seen in Fig.(11)). This allowed the CMB photons to travel freely, giving us the CMB that we

observe today. The photons were most likely to last scatter during the recombination epoch (a seen in Fig.(12)), decoupling from any interaction with matter.
We also saw in Tab.(II) that the event of last scattering most likely happened shortly after our given definition for recombination. We also saw that the Saha-solution in Fig.(10) quickly becomes a bad approximation outside it's regime.

3. MILESTONE III

In this Milestone, our goal will be to see how small fluctuations in the spacetime background and matter densities evolve into cosmological structures. We have until now only worked with a FLRW-metric for our spacetime, assuming that spacetime is flat and expanding. However, luckily for all life in the Universe, this is not quite true - not even on cosmological scales. The small inhomogeneties on our spacetime can be modeled by the interplay of small perturbations on our FLRW-metric, as well as small anisotropies in early matter fluids (photons, baryons, dark matter).

We will thus in this Milestone calculate the relevant cosmological perturbations. We give some justifications for the equations, but no full derivations.
You can find summaries for the all the equations in **Full system**, **Tight coupling**, and **Initial conditions**.

3.1. Theory

3.1.1. Metric perturbations

The Universe is mostly flat, but not quite. Due to small inhomogeneities from galaxy structures etc. (on a cosmological scale), we have to perturb this onto our original spacetime. Since we assumed that the Universe has FLRW-spacetime, we would have to perturb the FLRW-metric $\overline{g}_{\mu\nu}$. The perturbation is written

$$g_{\mu\nu} = \overline{g}_{\mu\nu} + h_{\mu\nu} \tag{51}$$

where $g_{\mu\nu}$ is our perturbed metric, and $h_{\mu\nu}$ is a small correction term to the FLRW-metric. All quantities that correspond to the background-metric will be denoted by a bar. Since this term is really small, we only keep the linear order of the perturbation. Choosing Newtonian gauge for $h_{\mu\nu}$ and stating the result, our new perturbed metric is

$$ds^2 = -(1+2\Psi)dt^2 + a^2(1+2\Phi)d\vec{r}^2. \tag{52}$$

To find Ψ and Φ, we must solve the Einstein equations, given by

$$G_{\mu\nu} = 8\pi G T_{\mu\nu}$$

where $G_{\mu\nu}$ is the Einstein-tensor, and $T_{\mu\nu}$ is the energy-momentum tensor given as

$$T^{\mu}{}_{\nu} = \frac{g}{(2\pi)^3}\int \frac{d^3\vec{p}}{\sqrt{-\det g}}\frac{p^\mu p_\nu}{p^0} f(x,p). \tag{53}$$

Since this is just a brute-force calculation, we will not do it here, but the results for Ψ and Φ are given directly in the summary Sec.(3 3.1 3.1.5).

3.1.2. Boltzmann-equations

Whenever we need to know the statistical behaviour of a thermodynamic system that is not in equilibrium, we need to write down the Boltzmann-equation to describe the evolution of the system. The Boltzmann equation is

$$\frac{df}{d\lambda} = C[f] \tag{54}$$

where f is the phase-space distribution, λ is an affine parameter related to the eigentime τ by $\lambda = a\tau + b$, and $C[f]$ is the collision term. Introducing phase-space coordinates (x^μ, p^μ) where x^μ is four-position and p^μ is four-momentum, we can write the Boltzmann-equation using the chain rule

$$\frac{\partial f}{\partial t}\frac{dt}{d\lambda} + \frac{\partial f}{\partial x^i}\frac{dx^i}{d\lambda} + \frac{\partial f}{\partial E}\frac{dE}{d\lambda} + \frac{\partial f}{\partial \hat{p}^i}\frac{d\hat{p}^i}{d\lambda} = C[f] \tag{55}$$

where we chose to expand in energy E and momentum direction $\hat{p}$ instead of momentum $\vec{p}$ for later convenience. In GR, the 3-momentum is defined via. $\vec{p}^2 \equiv g_{ij}p^i p^j$. We introduce the energy by using the energy-momentum relation $E^2 = m^2 + \vec{p}^2$, which together with the normalization of the four-momentum $p^2 = p_\mu p^\mu = -m^2$ (with $(-,+,+,+)$ signature) gives

$$g_{00}(p^0)^2 = -E^2 \Rightarrow p^0 = \frac{E}{\sqrt{1+2\Psi}}.$$

Since Ψ is a small perturbation, we can Taylor-expand

$$p^0 = \frac{E}{\sqrt{1+2\Psi}} \approx (1-2\Psi)E.$$

For the spatial components, we know $p^i \propto \hat{p}^i$ (or equivalently $p^i = A\hat{p}^i$) where $\hat{p}^i$ is the component momentum direction vector $\hat{p}$, satisfying $\hat{p}^i\hat{p}^j\delta_{ij} = 1$. We then have

$$\begin{aligned}
\vec{p}^2 &= g_{ij}p^i p^j \\
&= a^2(1+2\Phi)\delta_{ij}A^2\hat{p}^i\hat{p}^j \\
&= a^2(1+2\Phi)A^2, \\
\Rightarrow \quad A &= \frac{|\vec{p}|}{a\sqrt{1+2\Phi}}, \\
\Rightarrow \quad p^i &= \frac{|\vec{p}|\hat{p}^i}{a\sqrt{1+2\Phi}} \approx \frac{|\vec{p}|}{a}(1-2\Phi)\hat{p}^i,
\end{aligned}$$

using a Taylor-expansion in Φ. Using the geodesic equation

$$\frac{dp^\mu}{d\lambda} + \Gamma^\mu_{\alpha\beta} p^\alpha p^\beta = 0 \tag{56}$$

for $\mu = 0$ gives

$$\frac{dE}{d\lambda}(1-\Psi) - E\frac{d\Psi}{d\lambda} + \Gamma^0_{\alpha\beta} p^\alpha p^\beta = 0. \tag{57}$$

The Christoffel-symbols can easily be found from the metric $g_{\mu\nu}$, but we won't bother showing it here. Writing $\frac{d\Psi}{d\lambda} = (\partial_\mu \Psi) p^\mu$, approximating $\Gamma^0_{\alpha\beta} p^\alpha p^\beta$ and collecting $\frac{dE}{d\lambda}$ gives

$$\frac{dE}{d\lambda} \simeq -|\vec{p}|^2 \left[H(1-\Psi) + \frac{\partial \Phi}{\partial t} + \frac{E}{|\vec{p}|}\frac{\partial \Psi}{\partial x^i}\frac{\hat{p}^i}{a} \right]. \tag{58}$$

Now we want to use the Boltzmann-equation in Eq.(55). We neglect the last term on the LHS as it is second order in perturbation, while we are only interested in first order. Substituting Eq.(58) into Eq.(55) we have

$$\frac{df}{dt} \simeq \left[H(1-\Psi) + \frac{\partial \Phi}{\partial t} + \frac{E}{|\vec{p}|}\frac{\partial \Psi}{\partial x^i}\frac{\hat{p}^i}{a} \right] \frac{\partial f}{\partial E} - p^0 \frac{\partial f}{\partial t} - p^i \frac{\partial f}{\partial x^i}. \tag{59}$$

Now we will need to use this equation to get perturbations for baryons, dark matter and photons. We will not do the full derivations here due to length, but a detailed description is found at [7]. We will simply state the results with short explanations.

3.1.3. Photon tempterature perturbation

Since we are interested in the CMB-radiation, we want to find the fluctuations of the photon temperature due to the perturbed spacetime. We will simply consider the perturbed temperature $T = \overline{T}[1 + \Theta(x,p)]$. The collision term $C[f]$ in the Boltzmann-equation can be found as [7]

$$C[\Theta] = -p^2 \frac{\partial \overline{f}}{\partial p} n_e \sigma_T [\Theta_0 - \Theta + \hat{p} \cdot \vec{v}_b]. \tag{60}$$

The final result is

$$\frac{\partial \Theta}{\partial t} + \frac{ik\mu}{a}\Theta + \left(\frac{\partial \Phi}{\partial t} + \frac{ik\mu}{a}\Psi \right) = n_e \sigma_T \left[\Theta_0 - \Theta + i\mu v_b - \frac{3\mu^2 - 1}{4}\Theta_2 \right], \quad \mu \equiv \frac{\hat{p}\cdot\vec{k}}{k} \tag{61}$$

where we now have gone from position space x^i to Fourier-space with Fourier-modes k, and Θ_0 and Θ_2 is the monopole and quadrupole moment of the Θ distribution.

The next step would be to do a multipole expansion of Θ. We can decompose Θ as

$$\Theta(t,k,\mu) = \sum \frac{2\ell+1}{i^\ell} \Theta_\ell(t,k) P_\ell(\mu), \tag{62}$$

where Θ_ℓ are called multipoles of Θ, and P_ℓ are the Legendre polynomials. By orthogonality of Legendre polynomials, we can find the multipoles Θ_ℓ as

$$\Theta_\ell = \frac{i^\ell}{2} \int_{-1}^{1} \Theta(t,k,\mu) P_\ell(\mu) d\mu. \tag{63}$$

Plugging this into Eq.(61) and massage, we get to the expressions given in Sec.(3 3.1 3.1.5) and Sec.(3 3.1 3.1.6) switching from derivatives in t to x using $\frac{dt}{dx} = \frac{1}{H}$.

3.1.4. Density and velocity perturbations

For dark matter, things are kind of simple. Since dark matter is weakly interacting with standard-model particles, the collision term is zero such that the Boltzmann equation becomes

$$\frac{\partial f}{\partial t} + \frac{\partial f}{\partial x^i}\frac{P^i}{P^0} + \frac{\partial f}{\partial E}\frac{1}{P_0}\frac{dE}{d\lambda} = 0. \tag{64}$$

Since dark matter is non-relativistic at the times we are interested in and will only have a leading contribution from the monopole and dipole term, the evolution is fully characterized by the density $\delta_{\rm CDM}$ and velocity $v_{\rm CDM}$. The resulting equations are

$$\frac{\partial n_{\rm CDM}}{\partial t} + \frac{1}{a}\frac{\partial}{\partial x^i}(n v^i)_{\rm CDM} + 3 n_{\rm CDM}\left[H + \frac{\partial \Phi}{\partial t} \right] = 0, \tag{65}$$

$$\frac{\partial v^i_{\rm CDM}}{\partial t} + H v^i = -\frac{1}{a}\frac{\partial \Psi}{\partial x^i}, \tag{66}$$

where $n_{\rm CDM} = \overline{n}_{\rm CDM}[1 + \delta_{\rm CDM}] = \int \frac{d^3p}{(2\pi)^3} f$ is the number density of dark matter.

> Notice that we can recognize the equation for $n_{\rm CDM}$ as the continuity equation (conservation of mass) with additional cosmological spice, as this will soon be important. The same goes for $v_{\rm CDM}$, which could be recognized as the Euler equation (conservation of momentum).

Substituting and keeping only first order terms gives the equation for the density perturbation

$$\frac{\partial \delta_{\rm CDM}}{\partial t} + \frac{1}{a}\frac{\partial v^i_{\rm CDM}}{\partial x^i} + 3H\frac{\partial \Phi}{\partial t} = 0. \tag{67}$$

Now we need the corresponding equations for baryons. For baryons, the main interactions are Coulomb scattering

$$e^- + p^+ \leftrightharpoons e^- + p^+, \tag{68}$$

and Compton scattering

$$\begin{aligned} e^- + \gamma &\leftrightharpoons e^- + \gamma, \\ p^+ + \gamma &\leftrightharpoons p^+ + \gamma. \end{aligned} \tag{69}$$

Since the cross-section $\sigma \propto 1/m^2$ is suppressed by the mass squared, we can ignore the last interaction as the proton mass is much larger than the electron mass. The Coulomb-interaction is what couples electrons and protons, and due to the electric force being much larger than gravitational forces, the density fluctuations of electrons and protons are almost the same. Thus we define only two perturbation parameters $\delta_e = \delta_p \equiv \delta_b$ and $v_e = v_p \equiv v_b$.

Now comes an important part: since both the Coulomb and Compton interactions do not change the number of baryons - they are conserved, none of them will contribute to the continuity equation. Thus the same result for dark matter applies for baryons, and we can immediately write down the respective equation. Thus we get

$$\frac{\partial \delta_b}{\partial t} + \frac{1}{a}\frac{\partial v_b^i}{\partial x^i} + 3H\frac{\partial \Phi}{\partial t} = 0. \tag{70}$$

For v_b it is not just as easy, as we will get contributions to the Euler equation from Compton scattering, since momentum will transfer in between baryons and photons. I will state the result, which is derived in [7]

$$\frac{\partial v_b^i}{\partial t} + H v_b^i = -\frac{1}{a}\frac{\partial \Psi}{\partial x^i} + \frac{4\overline{\rho}_\gamma}{3\overline{\rho}_b}\tau'(3\Theta_1 + v_b). \tag{71}$$

These equations will be massaged, and translated from $t \to x$ in the summaries Sec.(3 3.1 3.1.5) and Sec.(3 3.1 3.1.6). For photons, the corresponding terms can be found using $T^0{}_0$ from the stress-energy tensor $T^\mu{}_\nu$ in Eq.(53). Then we have

$$T^0{}_0 = -\frac{g}{(2\pi)^3}\int d^3\vec{p}\, Ef = -\rho. \tag{72}$$

Writing $f = \overline{f} + \delta f$ we find

$$T^0{}_0 = \overline{T}^0{}_0 - \frac{g}{(2\pi)^3}\int d^3\vec{p}\, E\delta f.$$

With $\delta f = -p\Theta\frac{\partial \overline{f}}{\partial p}$ for photons we write

$$\begin{aligned} \frac{g}{(2\pi)^3}\int d^3\vec{p}E\delta f &= -\frac{g}{(2\pi)^3}\int d^3\vec{p}\Theta p^2\frac{\partial \overline{f}}{\partial p} \\ &= -\frac{g}{(2\pi)^3}\int d\Omega\int dp\Theta p^4\frac{\partial \overline{f}}{\partial p} \\ &= \frac{g}{(2\pi)^3}4\int d\Omega\Theta\int dp p^3\overline{f} \\ &= \frac{4}{4\pi}\int d\Omega\Theta\frac{g}{(2\pi)^3}\int dp 4\pi p^2\cdot p\overline{f} \\ &= -4\Theta_0\overline{\rho}_\gamma \end{aligned}$$

Thus we have

$$\left(T^0{}_0\right)_\gamma = -\overline{\rho}_\gamma(1 + 4\Theta_0) = -\overline{\rho}_\gamma(1 + \delta_\gamma). \tag{73}$$

Thus we now see that $\delta_\gamma = 4\Theta_0$. Similarly with the Euler-equation, we can show that $v_\gamma = -3\Theta_1$. This physically makes sense, as Θ_0 is the mean temperature of the photons - meaning the more/less photons we have, the higher/lower is the mean temperature.

3.1.5. The full system

There is essentially a lot of equations, so it might be a good idea to collect all of them in one small section. Here, the prime notation means $F' \equiv \frac{d}{dx}F$, where $x = \ln(a)$ just as before. All quantities in the equations are given in previous Milestones.

Photon tempterature multipoles:

$$\begin{aligned} \Theta_0' &= -\frac{ck}{\mathcal{H}}\Theta_1 - \Phi', \\ \Theta_1' &= \frac{ck}{3\mathcal{H}}\Theta_0 - \frac{2ck}{3\mathcal{H}}\Theta_2 + \frac{ck}{3\mathcal{H}}\Psi + \tau'\left[\Theta_1 + \frac{1}{3}v_b\right], \\ \Theta_2' &= \frac{2ck}{5\mathcal{H}}\Theta_1 - \frac{3ck}{5\mathcal{H}}\Theta_3 + \frac{9}{10}\tau'\Theta_2, \\ \Theta_\ell' &= \frac{\ell ck}{(2\ell+1)\mathcal{H}}\Theta_{l-1} - \frac{(\ell+1)ck}{(2\ell+1)\mathcal{H}}\Theta_{\ell+1} + \tau'\Theta_\ell, \\ &\qquad\qquad 3 \le \ell < \ell_{\max}, \\ \Theta_\ell' &= \frac{ck}{\mathcal{H}}\Theta_{\ell-1} - c\frac{\ell+1}{\mathcal{H}\eta(x)}\Theta_\ell + \tau'\Theta_\ell, \qquad \ell = \ell_{\max}. \end{aligned} \tag{74}$$

Cold dark matter and baryons:

$$\begin{aligned} \delta_{\rm CDM}' &= \frac{ck}{\mathcal{H}}v_{\rm CDM} - 3\Phi', \\ v_{\rm CDM}' &= -v_{\rm CDM} - \frac{ck}{\mathcal{H}}\Psi, \\ \delta_b' &= \frac{ck}{\mathcal{H}}v_b - 3\Phi', \\ v_b' &= -v_b - \frac{ck}{\mathcal{H}}\Psi + \tau' R(3\Theta_1 + v_b). \end{aligned} \tag{75}$$

Metric perturbations:

$$\begin{aligned}\Phi' =\ & \Psi - \frac{c^2k^2}{3\mathcal{H}^2}\Phi + \frac{H_0^2}{2\mathcal{H}^2} \\ & \cdot[\Omega_{\rm CDM0}e^{-x}\delta_{\rm CDM} + \Omega_{b0}\delta_b e^{-x} + 4\Omega_{\gamma 0}e^{-2x}\Theta_0], \\ \Psi =\ & -\Phi - \frac{12H_0^2}{c^2k^2}\Omega_{\gamma 0}\Theta_2 e^{-2x}.\end{aligned} \tag{76}$$

3.1.6. Tight coupling regime

Recall that in Milestone 2, we had to divide the evolution into two regimes due to the general differential equations being unstable at early times. Take for example the equation for v_b' in Eq.(75). The term $\tau'(3\Theta_1 + v_b) = \tau'(v_b - v_\gamma)$ causes trouble, since $|\tau'| \gg 1$ will be huge as seen in Fig.(11) from Milestone 2. Then small errors in velocity will become huge errors in the equation. This also goes for Θ_1 in Eq.(74). Therefore we need separate equations for early times. This early regime is what we call the *tight coupling regime*, due to baryons and photons being tightly coupled. Due to the high efficiency of Compton scattering in Eq.(69), all the higher order multipoles become negligible. Thus we only really need to consider the two first multipoles, Θ_0 and Θ_1.
One can show that in the tight coupling regime,

$$(3\Theta_1 + v_b) \propto \frac{1}{\tau'} \propto \eta$$

is a good approximation, since $\tau' \propto \frac{1}{a}$ and $\eta \propto a$ in a radiation dominated Universe. This gives us

$$\frac{d^2}{d\eta^2}(3\Theta_1 + v_b) \approx 0 \Rightarrow [3\Theta_1 + v_b]'' \approx -\frac{\mathcal{H}'}{\mathcal{H}}[3\Theta_1 + v_b]',$$

and defining $q \equiv [3\Theta_1 + v_b]' \rightarrow \Theta_1' = \frac{q - v_b'}{3}$ with $\Theta_2' \sim 3\Theta_2 \ll \Theta_0$ gives the resulting equation for q below.
Then, solving for $\tau'(1+R)\,[3\Theta_1 + v_b]$ gives

$$\tau'(1+R)\,[3\Theta_1 + v_b] = \frac{q - \frac{ck}{\mathcal{H}}(\Theta_0 - 2\Theta_2) + v_b}{1+R},$$

which can be substituted into v_b' to give

$$v_b' = \frac{1}{1+R}\left[-v_b - \frac{ck}{\mathcal{H}}\Psi + R(q + \frac{ck}{\mathcal{H}}(-\Theta_0 + 2\Theta_2) - \frac{ck}{\mathcal{H}}\Psi)\right].$$

All the tight-coupling equations are given below.

Tight coupling equations :

$$\begin{aligned} q_1 &= \frac{-[(1-R)\tau' + (1+R)\tau''](3\Theta_1 + v_b)}{(1+R)\tau' + \frac{\mathcal{H}'}{\mathcal{H}} - 1}, \\ q_2 &= -\frac{\frac{ck}{\mathcal{H}}\Psi + (1 - \frac{\mathcal{H}'}{\mathcal{H}})\frac{ck}{\mathcal{H}}(-\Theta_0 + 2\Theta_2) - \frac{ck}{\mathcal{H}}\Theta_0'}{(1+R)\tau' + \frac{\mathcal{H}'}{\mathcal{H}} - 1}, \\ q &= q_1 + q_2, \\ v_b' &= \frac{\left[-v_b - \frac{ck}{\mathcal{H}}\Psi + R(q + \frac{ck}{\mathcal{H}}(-\Theta_0 + 2\Theta_2) - \frac{ck}{\mathcal{H}}\Psi)\right]}{1+R}, \\ \Theta_1' &= \frac{1}{3}(q - v_b'), \\ \Theta_2 &= -\frac{20ck}{45\mathcal{H}\tau'}\Theta_1, \\ \Theta_\ell &= -\frac{\ell}{2\ell+1}\frac{ck}{\mathcal{H}\tau'}\Theta_{\ell-1}, \qquad \ell > 2. \end{aligned} \tag{77}$$

From Eq.(77) it becomes more evident that the higher order multipoles are negligible in the tight couple regime, as $\Theta_2 \propto (\tau')^{-1}, \Theta_3 \propto (\tau')^{-2}, \ldots, \Theta_k \propto (\tau')^{-(k-1)}$, and $|\tau'| \gg 1$ is huge in the early Universe.

3.1.7. Inflation

There are several problems connected to the early stages of the universe. One of these problems is that CMB radiation is measured to have the same temperature to high precision in any direction. This means that light on the opposite sides of the Universe have the same temperature. For this to happen, the areas in which the light came from need to be in contact for a longer period of time so that they can obtain thermal equilibrium. However, at early times these areas were not causally connected, as the Universe had not yet expanded enough for these areas to causally communicate.
This is called the *Horizon problem*, and one possible fix is to introduce an epoch called *inflation*. Inflation then suggests that these regions actually were close together before inflation - and not causally disconnected, such that they are in thermal equilibrium. Then during the inflation epoch, the Universe expands exponentially fast in a short period of time in such a way that matches the Universe today.

One way to model inflation is to introduce a new scalar quantum field $\phi(x)$ with some self-interaction potential V, called the *inflaton field*. For inflation to have exponential growth of the scalefactor, the inflaton field must model a fluid with equation of state $w \simeq -1$. The equation of state for such a particle is

$$w = \frac{\frac{1}{2}\dot{\phi}^2 - V}{\frac{1}{2}\dot{\phi}^2 + V} \simeq -1,$$

with $\dot{\phi} \equiv \frac{d\phi}{dt}$, meaning that we must have the kinetic energy $\frac{1}{2}\dot{\phi}^2 \ll V$. This is called *slow roll*, due to the field "slowly rolling down its potential". At the bottom of the potential where $V \approx 0$, we get $w \approx 1$, meaning the inflation has stopped. We essentially want to connect this period to initial conditions for our system. One important combination of metric perturbations is the curvature perturbation $\mathcal{R}$, derived in [7] as

$$\mathcal{R} = \frac{ik_i \delta T^0_{\ i}}{k^2(\rho + P)} - \Psi = \Phi + \frac{\mathcal{H}^2(\Phi' - \Psi)}{4\pi G a^2(\overline{\rho} + \overline{P})}, \tag{78}$$

in Newtonian gauge, and $T^i_{\ 0} = g^{i\nu}\partial_\nu\phi\partial_0\phi$ is the spatial part of the stress-energy tensor of the inflaton field. In momentum-space, we then get $\delta T^i_{\ 0} = \frac{ik_i}{a^2}\dot{\phi}\delta\phi$. Additionally, it satisfies

$$\frac{d\mathcal{R}}{dt} \approx 0, \quad k \ll \mathcal{H} \Leftrightarrow k\eta \ll 1.$$

In other words, this is a conserved quantity for any mode that is outside of the Horizon (recall $\frac{1}{k} \sim \lambda$ where λ is the length scale in position). This makes it possible to connect the initial conditions in the early Universe to what was generated in inflation. Since $\mathcal{R}$ is conserved outside the horizon, $k\eta \ll 1$, we can connect the predictions for the fluctuations put up by inflation to what we should put as the initial conditions for Φ.

Now we only need to relate fluctuations in the metric to density perturbations of the matter.

3.1.8. Initial conditions

We have all the evolutionary equations for the system, and now we need initial conditions. We need to make some assumptions. We assume adiabatic initial conditions, meaning

$$\frac{n_i}{n_\gamma} = \frac{\overline{n}_i}{\overline{n}_\gamma}$$

for i, j being indices for every species, and n the number density. Another way to phrase this is that density fluctuations were initially present in the Universe. Since $\overline{\rho}_i(a) \propto 1/a^{3(1+w_i)}$ we can find

$$\rho_i(x, a) = \overline{\rho}_i(a + \delta a(x)) \simeq \overline{\rho}_i(a)(1 - 3(1 + w_i)\delta a(x)/a),$$

which gives

$$\frac{\delta_i}{1 + w_i} = \frac{\delta_j}{1 + w_j},$$

and further implies (using $w_\gamma = \frac{1}{3}, w_{\rm CDM} = w_b \approx 0$)

$$\frac{3}{4}\delta_\gamma = \delta_b = \delta_{\rm CDM} = 3\Theta_0.$$

We still need Ψ and Φ. The metric perturbations evolve slowly outside of the horizon, so we have $\Psi' \approx 0$, $\Phi' \approx 0$. From the Poisson equation we get

$$2\Theta_0 \simeq -\Psi,$$

which relates $\delta_b = \delta_{\rm CDM} = -\frac{3}{2}\Psi$. The equation for $v'_{\rm CDM}$ in Eq.(75) can be written as

$$(v_{\rm CDM}a)' = -\frac{cka}{\mathcal{H}}\Psi \xrightarrow{\int dx} v_{\rm CDM} = Ce^{-x} - \frac{ck}{2\mathcal{H}}\Psi,$$

by multiplying the equation by a and using that $a' = a$. Since the C-term is a decaying mode, it can be ignored. This gives the initial condition $v_{\rm CDM} = -\frac{ck}{2\mathcal{H}}\Psi$. The same analysis can be done for Θ_1 and v_b, giving

$$\Theta_1 \simeq \frac{ck}{6\mathcal{H}}\Psi,$$
$$v_b \simeq -\frac{ck}{2\mathcal{H}}\Psi.$$

From Eq.(74) we also find

$$\Theta_2 = -\frac{20ck}{45\mathcal{H}\tau'},$$
$$\Theta_\ell \simeq -\frac{\ell}{2\ell + 1}\frac{ck}{\mathcal{H}\tau'}\Theta_{\ell-1} \text{ for } \ell. > 2$$

Which both are non-trivial results. Since our set of equations are linear, we can choose any normalization of the system before solving, and plug in correct normalization after solving. For a mode outside of the horizon in the radiation dominated era we have

$$\mathcal{R} \simeq \Phi - \frac{1}{2}\Psi.$$

The relation between Ψ and Φ is given in [7] as

$$\Phi + \Psi \simeq -\frac{2f_\nu}{5}\Psi,$$

with $f_\nu = \frac{\Omega_\nu}{\Omega_\gamma + \Omega_\nu} = 0$, since there is no neutrinos in this project. Choosing normalization with $\mathcal{R} = 1$ we get

$$\Psi \simeq -\frac{1}{\frac{3}{2} + \frac{2f_\nu}{5}} = -\frac{2}{3},$$
$$\Phi \simeq -\left(1 + \frac{2f_\nu}{5}\right)\Psi = -\Psi.$$

Similarly, we can derive initial conditions for Θ_ℓ, but we will just state the result. All initial conditions are summarized in the box below.

Initial conditions :

$$\begin{aligned}
\Psi &= -\frac{2}{3}, \\
\Phi &= -\Psi, \\
\delta_{\rm CDM} &= \delta_b = -\frac{3}{2}\Psi, \\
v_{\rm CDM} &= v_b = -\frac{ck}{2\mathcal{H}}\Psi, \\
\Theta_0 &= -\frac{1}{2}\Psi, \\
\Theta_1 &= \frac{ck}{6\mathcal{H}}\Psi, \\
\Theta_2 &= -\frac{20ck}{45\mathcal{H}\tau'}\Theta_1, \\
\Theta_\ell &= -\frac{\ell}{2\ell+1}\frac{ck}{\mathcal{H}\tau'}\Theta_{\ell-1}.
\end{aligned} \tag{79}$$

The initial conditions for the multipoles $\ell \geq 2$ are the same equations for the multipoles in the tight coupling regime.

3.2. Implementation, numerical methods and tests

The implementation of this section will be very similar to that of the previous Milestone, but now with coupled equations. As previously, we want to solve the differential equations using the ODESolver. Since we now have a set of coupled ODEs, we can write our equations on vector form

$$\frac{d\vec{Y}}{dx} = \vec{A}(\vec{Y})$$

where $\vec{Y}$ is implemented as an array with the quantities we want to solve for. This summarizes the equations from the theory section, where $\vec{A}(\vec{Y})$ is the RHS of the ODE, which is implemented and solved.

The only thing we have to consider when solving the ODEs is whether we are in the tight coupling regime or not. As mentioned in Sec.(3 3.1 3.1.6), we need to handle the tight coupling regime due to $|\tau'| \gg 1$ huge at early times. Since recombination happens around $x \approx -7$, we expect the tight coupling regime to end before $x \approx -7$ since photons and matter have decoupled by this time. Thus one of the tests we will use is to set x to some threshold value in which we end tight coupling. We ideally want to end tight coupling as soon as possible to start solving for the full system, and choose a value for x which is close to where we still have a numerically stable solution. This could be computationally more heavy. We choose the threshold value to be $x = -8.3$, which is just a convenient choice which optimize the computation speed without changing the data too much.

There are still some other tests to use. To have a fail-safe we will also adopt the conditions from [8], stating that we still are in the tight coupling regime as long as

$$|\tau'| > 10, \quad |\tau'| > \frac{10ck}{\mathcal{H}}.$$

Whenever any of these three conditions are broken, we will break from solving the tight coupling equations and start solving the full system. It is important that we use the last values that we found in the tight coupling regime as initial values when switching to solve the full regime, to make sure the solutions are connected. Another important thing to keep in mind is that the order in which the equations are solved matters, and if one gets this wrong one will end up with nonsense.

3.3. Results and discussion

In Fig.(13a) we can see the density perturbation for CDM and baryons, for three different Fourier-modes $k = 0.1, 0.01, 0.001/\text{Mpc}$. Each mode corresponds to a different scale in real space, roughly corresponding to $\lambda \sim \frac{\text{Mpc}}{k}$, giving $\lambda \sim 10, 100, 1000\text{Mpc}$. For reference, galaxies are usually somewhere in $1-100\text{kpc}$ in diameter, while the observable Universe is $\sim 28.5\text{Gpc}$ in diameter.

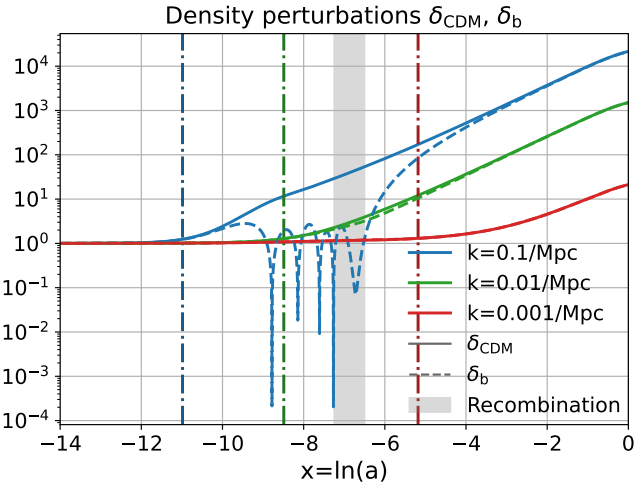

(a) Evolution of density perturbations for CDM and baryons.

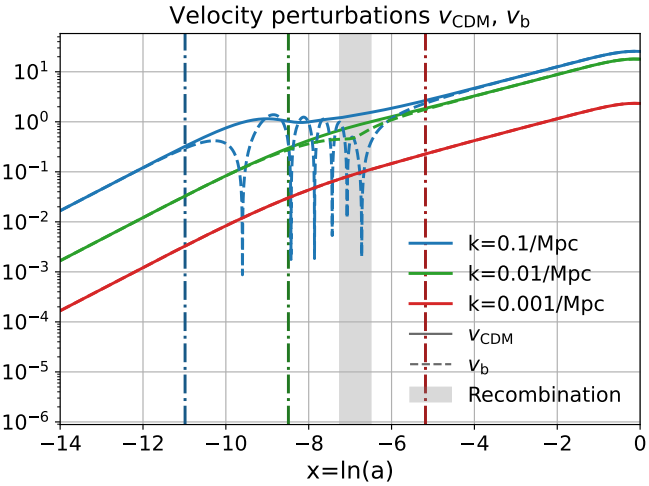

(b) Evolution of velocity perturbations for CDM and baryons.

FIG. 13: Evolution of the absolute value of Fourier-transformed density and velocity perturbations for CDM and baryons. The dot-dashed line is where horizon-crossing roughly happens, each for their respective k-value. The grey strip signifies recombination/the width of the visibility function $\tilde{g}$.

The dot-dashed lines represent roughly where horizon-crossing happens, i.e where the scale and horizon are approximately equal, $\eta \sim \lambda$. This means that regions on the given scale are able to interact, as they now are causally connected. Now we have to keep in mind while interpreting the graphs that these are Fourier-transformed quantities. Roughly speaking, oscillations in Fourier-space correspond to propagation in position-space. This can most easily be seen from Fourier-transforming the wave-equation, which describes a propagating wave. Then

$$\frac{\partial^2 f}{\partial t^2} = \frac{1}{c^2}\nabla^2 f \longleftrightarrow \frac{\partial^2 \tilde{f}}{\partial t^2} = -\frac{k^2}{c^2}\tilde{f} = -\omega^2 \tilde{f},$$

which is the equation for a harmonic oscillator. Thus oscillations in the Fourier-space corresponds to propagation in real-space. In Fig.(13a) we can see the absolute values of the density perturbations, meaning that the graph for $\delta_b, k = 0.1/\text{Mpc}$ in $x \in [-10, -6]$ are oscillations in Fourier-space. Also, since we only Fourier-transformed in position, $\delta(t, x)$ will increase in time if $\delta(t, k)$ does.

We would now like to interpret Fig.(13a) to get some physics from it. At the early times when $x \in [-15, -12]$, nothing happens to any of the graphs. This is because the horizons of different structures are not causally connected - nothing is interacting on the given scales. Now, for simplicity, let's only look at the $k = 0.1/\text{Mpc}$ graph in Fig.(13a). Around $x = -11$ (horizon crossing) the mode enter the horizon, which is during radiation domination. Due to gravity the baryons and dark-matter starts to cluster, causing the overdensities to grow. These overdense regions now contains baryons, dark matter and photons. Dark matter is not coupled to anything, and thus evolves on its own - only fighting the expansion of the Universe. The baryons however are coupled to photons, and will experience radiation pressure that keeps the overdensity from increasing by pushing the clustering baryons outwards.
The interplay between pressure and gravity can first be seen around $x \approx -9$, where the Fourier-baryon overdensity suddenly drops and starts to oscillate. This is because photons drag baryons with them, making radially propagating waves of baryon-photon plasma seen as oscillations in the Fourier-space (these are called *baryon acoustic oscillations*). This keeps on going until $x \approx -6.5$, where the Fourier-baryon overdensity stops oscillating, and starts to increase again. This is due to the photons *decoupling* from the baryons during recombination. Recall from Sec.(2) that we in Tab.(II) found that last scattering happens at $x \approx -7$. This means photons no longer will drag the baryons with them as the photons have decoupled from matter, leaving behind shells of baryonic matter. The distance in which these shells could be found is described by the *sound horizon* given in Eq.(50). The decoupling of photons is manifestly seen in Fig.(13a) as the oscillations stopping. During this period the dark matter density has increased, and baryons will now start to cluster in the gravitational wells made by the dark matter.

Now, the previous discussion was only for the smallest scale, $k = 0.1/\text{Mpc}$. For the larger scales, we can see that the densities starts to evolve sooner. As already mentioned, this is due to the horizons of structures not being large enough to causally interact. Since the horizons keep expanding, this will eventually happen for larger scales, but later in time than for smaller scales. This also means that more time passes before the larger modes enter the horizon. For the intermediate mode $k = 0.01/\text{Mpc}$, the mode enters the horizon around

radiation-matter equality, evolving during recombination such that the baryon density slightly deviates from the dark matter. However, before the baryons have time to evolve sufficient density, recombination has already happened and no oscillatory behaviour is therefore displayed. For the largest scale, $k = 0.001$/Mpc, we can see that the baryon-density immediately follows the dark matter density, as the baryons will cluster in gravitational wells made by the dark matter. .

Notice that for the velocity perturbations (bulk velocity) in Fig.(13b), we can see that the shape is similar to that of Fig.(13a). We observe that whenever the overdensity crosses zero, we reach a maxima/minima for the bulk velocity, and vice versa. This is what one would expect from a harmonic oscillator.

In Fig.(14) we can see the the Fourier-transformed density and velocity perturbations of the photons for each $k = 0.1, 0.01, 0.001$/Mpc.

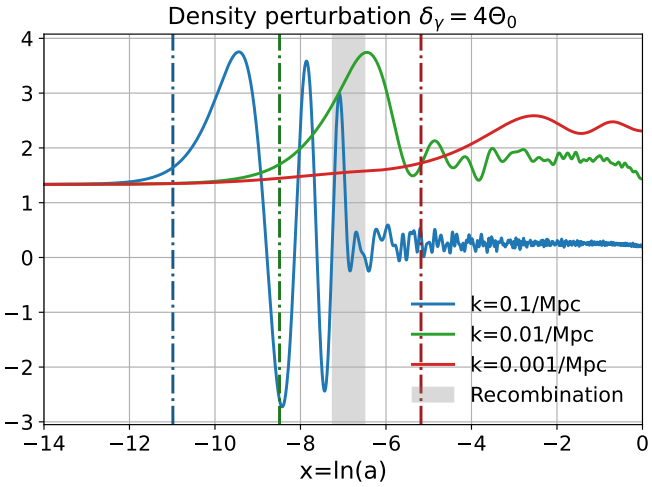

(a) Evolution of density perturbation for photons.

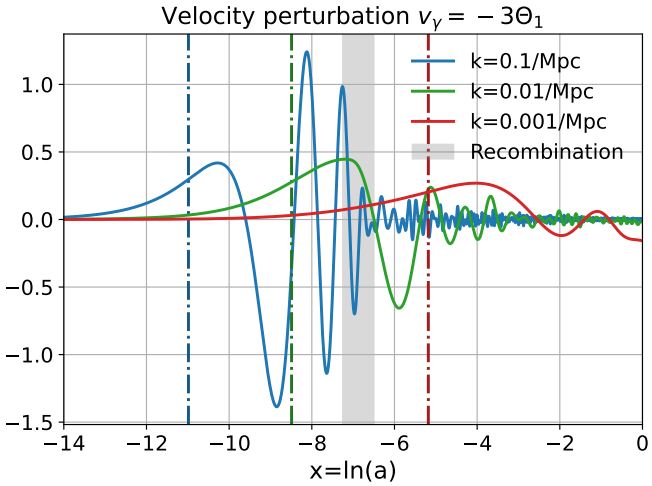

(b) Evolution of velocity perturbation for photons.

FIG. 14: Evolution of the Fourier-transformed density and velocity perturbations for photons. The dot-dashed line is where horizon-crossing roughly happens, each for their respective k-value. The grey strip signifies recombination/the width of the visibility function $\tilde{g}$.

Similarly to the baryons, we can see that the photons follow a oscillatory behaviour. This behaviour of the photon overdensity and bulk velocity is compared with those of baryons in Fig.(15), Fig.(16) and Fig.(17), where we can clearly see that the photons follow a similar evolution as baryons, since they are coupled. To avoid too much repetition, I refer to the discussion of the baryon overdensity, as photons and baryons are tightly coupled until recombination. Particularly interesting is the bulk velocity, where we see that photons and baryons follow each other identically. This further verifies that the photons drag the baryons with them, causing them to have the same bulk velocity at the same time during tight coupling - they move as one fluid.

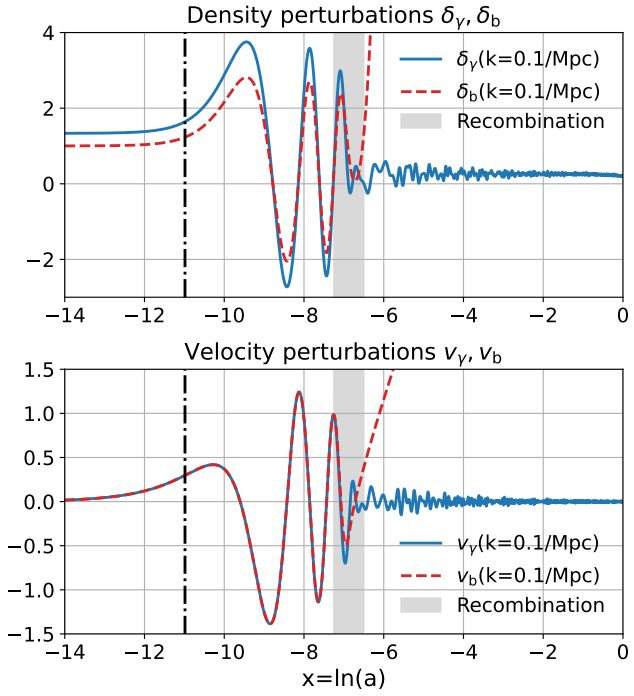

FIG. 15: Evolution of the Fourier-transformed density and velocity perturbations for photons and baryons at $k = 0.1$/Mpc plotted together. The dot-dashed line is where horizon-crossing roughly happens, each for their respective k-value. The grey strip signifies recombination/the width of the visibility function $\tilde{g}$. We can clearly see the tight coupling between photons and baryons until recombination.

This continues until recombination, where photons decouple from matter and their evolution differ. As previously discussed, the baryons start to cluster due to gravity. For the photons, they now travel freely through the Universe. We can still see fluctuating behaviour in the overdensity and bulk velocity of the photons, since the free electron density is small but non-zero after recombination. At larger modes, we still see some oscillatory behaviour for a small amount of time after recombination. This translates to photons freely propagating through space, which at larger scales naturally is seen later in time.

Additionally, we notice that the overdensities tend to drop when approaching $x = 0$. This is best seen on the larger scales, as in Fig.(14a) for $k = 0.01$ or in Fig.(19) which we yet have to discuss. Recall that we discovered in Milestone 1 that the Universe starts to accelerate when $\Omega_\Lambda \approx \frac{1}{3}$, which happens at $x \approx 0$. Thus the acceleration of the Universe stretches space between the particles, causing the overdensity to stop growing.

Lastly, we notice that δ_γ in Fig.(14a) does not eventually end up oscillate around $\delta_\gamma = 0$, which would be expected for a perturbation around a mean. This is due to Θ_0 not being the *effective* temperature, which would be $\Theta^{\text{eff}} = \Theta_0 + \Psi$. We will not consider this further here.

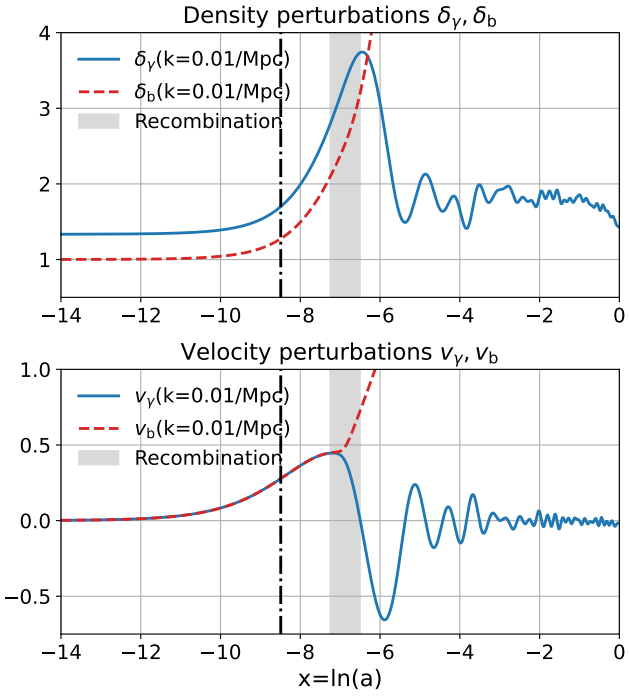

FIG. 16: Evolution of the Fourier-transformed density and velocity perturbations for photons and baryons at $k = 0.01$/Mpc plotted together. The dot-dashed line is where horizon-crossing roughly happens, each for their respective k-value. The grey strip signifies recombination/the width of the visibility function $\tilde{g}$. We can clearly see the tight coupling between photons and baryons until recombination.

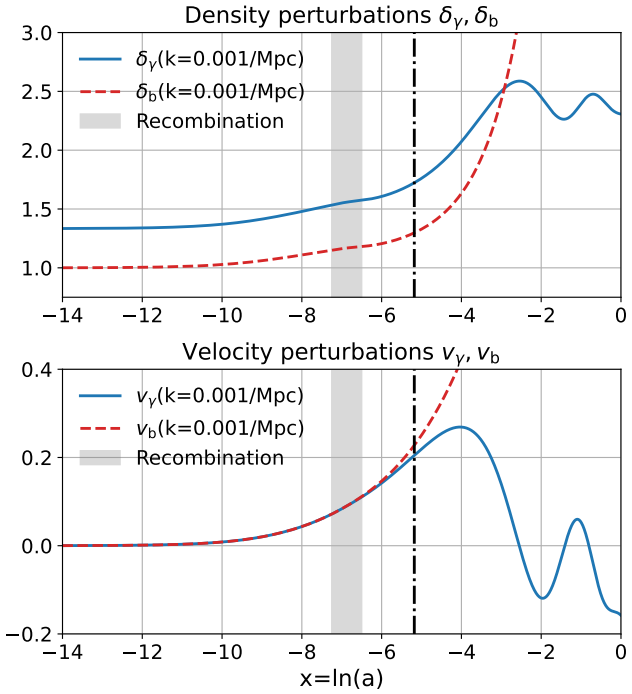

FIG. 17: Evolution of the Fourier-transformed density and velocity perturbations for photons and baryons at $k = 0.001$/Mpc plotted together. The dot-dashed line is where horizon-crossing roughly happens, each for their respective k-value. The grey strip signifies recombination/the width of the visibility function $\tilde{g}$. We can clearly see the tight coupling between photons and baryons until recombination.

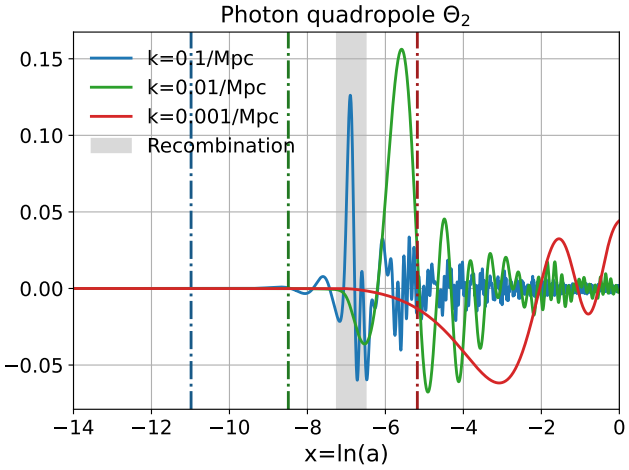

FIG. 18: Evolution of the Fourier-transformed photon dipole Θ_2. The dot-dashed line is where horizon-crossing roughly happens, each for their respective k-value. The grey strip signifies recombination/the width of the visibility function $\tilde{g}$.

In Fig.(18) we can see the quadrupole term for the photon temperature perturbation. The quadropole represents a higher order correction to the temperature fluctuations of the CMB photons. As opposed to Fig.(14a) and Fig.(14b), the evolution of Θ_2 starts in later times. This should be no surprise. Recall that during tight coupling/early times, only Θ_0 and Θ_1 are really apparent as the high efficiency of Compton scattering washes out all higher order multipoles due to a high density of free electrons. Thus when recombination happens, photons and baryons are no longer tightly coupled, which enables larger modes of the photon multipoles to evolve.

In Fig.(19) we can see the gravitational potential Φ, and in Fig.(20) the sum $\Phi + \Psi$. Let us first discuss Fig.(19). First we notice that the potential at all scales remain constant, due to having too small horizons to make them be affected by causal physics. Thus they remain at their initial values. When we reach the event of horizon crossing, the gravitational potential experiences a sudden drop. One might naively think that this is wrong, as baryons and dark matter already have started to cluster in this period of time. However, we are still in the radiation dominated era, meaning that radiation pressure from the photon-baryon fluid is counteracting gravitational forces - making the potential smaller. From Fig.(13a) we can see that for $k = 0.1$/Mpc both δ_{CDM} and δ_b are growing during $x \in [-12, -9]$, which we see in Fig.(19) is when the gravitational potential drops. After $x = -9$ (around $x \approx -8$), we see that δ_b starts to oscillate, which we can connect to the small oscillation of Φ during the same period of time. Around $x \approx -8$ we transition from the radiation dominated era to the matter dominated era. We see that all three modes in Fig.(19) flattens out around $x \approx 6$, due to matter domination. Around $x \approx 0$, we can also see a clear drop in Φ, caused by acceleration of the Universe during DE domination.

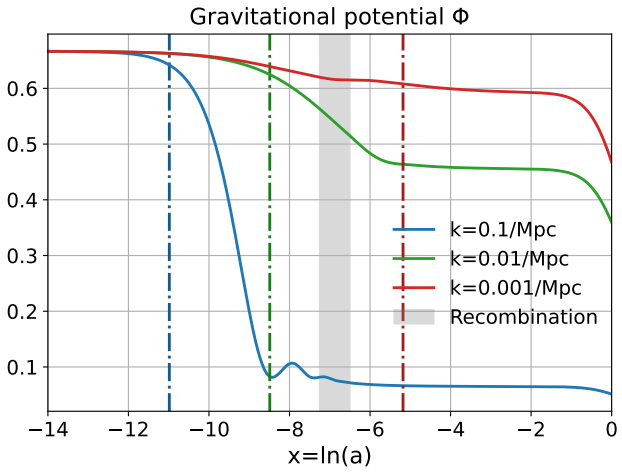

FIG. 19: Evolution of the Fourier-transformed potential Φ. The dot-dashed line is where horizon-crossing roughly happens, each for their respective k-value. The grey strip signifies recombination/the width of the visibility function $\tilde{g}$.

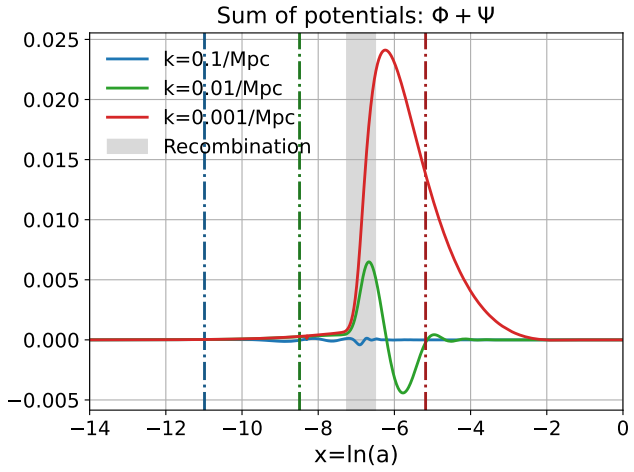

FIG. 20: Evolution of the Fourier-transformed anisotropy of the Universe. The dot-dashed line is where horizon-crossing roughly happens, each for their respective k-value. The grey strip signifies recombination/the width of the visibility function $\tilde{g}$.

Now it is time to discuss Fig.(20). As previously mentioned in Sec.(3 3.1), we have chosen to work in a Newtonian gauge when doing the metric perturbations. As long as we have an isotropic and homogenous Universe, the stress-energy tensor must be rotationally invariant under spatial rotations. Essentially, this gives us that $T_{\mu\nu} = \text{diag}(\rho, P, P, P)$ in a local rest frame, meaning that we don't have any anisotropic stress ($T_{ij} = 0$, $i \neq j$).

Inserting the stress-energy tensor for a perfect fluid into the Einstein equations with Newtonian gauge then gives $\Psi = -\Phi$, in which we would expect $\Phi + \Psi = 0$ at all times. However, we see in Fig.(20) that this is not the case at all times (it is really never the case, but way more present at some times than other). Thus the assumption of isotropy is wrong, meaning that we must have an anisotropy in the stress-energy during this period (being mainly in the matter-dominated era). This is indeed what Eq.(76) tells us, where we have an additional term related to the photon quadropole Θ_2. This equation essentially reads

$$\Phi + \Psi \propto \frac{\Theta_2}{k^2} e^{-2x},$$

and we see that for smaller scales (larger values of k), this effect is less present as seen in Fig.(20). We also see that this term will get smaller in increasing values for x.

Now, what causes this anisotropy? After recombination, baryons and dark matter start to cluster, sourcing gravitational wells throughout the Universe. Since the photons by this time are freely travelling, they will fall into the gravitational wells - getting blueshifted, and climb out again - getting redshifted. Since the gravitational wells still evolve, the photon might not get back the same amount of energy that it entered with. The gravitational wells cause anisotropies in spacetime, causing the fluctuating shifts in the photons - manifested as Θ_2 in Eq.(76) as "sourcing" anisotropies (it is really the other way around). Later the effect vanishes due to the expansion of the Universe, causing the gravitational wells to be further apart and making it less likely for photons to fall into them. These anisotropies eventually causes the formation of structures in the Universe, giving us the Universe as we know it today.

3.4. Conclusions

In the early Universe, nothing interacted due to the horizon being to small to causally interact with other objects. As the horizon grows, different scale modes starts to enter the horizon - enabling causal physics.

For the modes at scales in which the baryon overdensity grew sufficiently large before recombination, we observed baryon acoustic waves. This happened because baryons and dark matter started to cluster, trapping the photons inside overdense regions. Since dark matter weakly interacts with the standard model, only the baryons feel the radiation pressure exerted by the photons. The photons then drag the baryons with them, resulting in radially propagating waves of baryons being tightly coupled to photons - a baryon-photon plasma moving as one fluid. Then recombination happens, making the photons decouple from matter, leaving the baryons behind in shells. Then baryons and dark

matter start to cluster again, causing a larger amount of anisotropy in the Universe - sourcing gravitational wells. The now freely travelling photons then fall into these gravitational wells - causing blueshift, and climbs out again - causing redshift. This causes fluctuations in the photon temperature. The anisotropy and temperature fluctuations then dissipate due to the expansion of the Universe, causing larger distances between gravitational wells.

For the modes at scales in which the baryon overdensity did not grow sufficiently large before recombination, we never observed any baryon acoustic oscillations. This is because the photons had already decoupled from matter before the mode entered the horizon. Thus the baryons and dark matter continue to cluster together.

4. MILESTONE IV

In this Milestone we give the final result of the CMB power spectrum, both for photons and matter. We treat initial perturbations as Gaussian random fields, encapsulating the statistical nature of the Universe and the power spectrums. We also discuss the intrinsic statistical uncertainty of the Universe, and connects this to the CMB power spectrum. We find that the matter power spectrum estimates an upper bound for the size-scale cosmological structures in the Universe can have.

4.1. Theory

4.1.1. Gaussian random fields

A random variable x is fully determined from its probability distribution function (PDF) $f(x)$. For multiple gaussian random variables $x_1, x_2, ..., x_n$, we have the PDF

$$f(x_1, \dots, x_n) = \frac{1}{(2\pi)^{n/2}|\det \xi|^{1/2}} e^{-\frac{1}{2}x^T \xi x},$$

where

$$\xi_{ij} \equiv \langle x_i x_j \rangle = \prod_{k=1}^{n} \int_{-\infty}^{\infty} dx_k \; f(x_1, \dots, x_n) x_i x_j$$

is the two point correlation function, giving the correlation between the value of the random gaussian field between x_i and x_j. If all x_i's are independent, ξ will be a diagonal matrix, and the PDF is a product between 1D gaussians. Going to the continuum, we have $\xi = \langle x(\vec{q}_i)x(\vec{q}_j)\rangle$ where $\vec{q}$ is some spatial coordinates. Using the cosmological principle, we should only have $\xi = \xi(r_{ij})$ where $\vec{r}_{ij} = \vec{q}_j - \vec{q}_i$, $r_{ij} = |\vec{r}_{ij}|$, since the Universe is homogeneous and isotropic. Going to Fourier-space, we can express the correlation function as

$$\begin{aligned} C_{ij} = \langle \hat{x}(\vec{k}_i)\hat{x}^*(\vec{k}_j)\rangle &= \int d^3q_a d^3q_b e^{-ik_i q_a + ik_j q_b} \langle x(\vec{q}_a)x(\vec{q}_b)\rangle \\ &= (2\pi)^3 \delta(\vec{k}_i - \vec{k}_j) P(k_i), \end{aligned}$$

where $P(\vec{k}_i) = \int d^3r e^{i\vec{k}_i \cdot \vec{r}} \xi(\vec{r})$ is the *power spectrum*, which basically is the two point correlation function in Fourier-space. A big advantage of going to Fourier-space, is that the correlation function becomes diagonal because of $\delta(\vec{k}_i - \vec{k}_j)$, meaning that the PDF in Fourier-space becomes

$$\begin{aligned} f(\hat{x}(\vec{k}_1), \dots, \hat{x}(\vec{k}_n)) &= \frac{\exp\left[-\frac{1}{2}\sum_i \frac{|\hat{x}(\vec{k}_i)|^2}{P(k_i)}\right]}{(2\pi \prod_i P(k_i))^{n/2}} \\ &= \prod_i \frac{1}{\sqrt{2\pi P(k_i)}} \exp\left[-\frac{1}{2}\frac{|\hat{x}(\vec{k}_i)|^2}{P(k_i)}\right]. \end{aligned}$$

which is a product of 1D-Gaussian distributions - being another good reason for working in Fourier-space.

4.1.2. Power spectrums

The CMB encloses the sky, giving it a spherical shape. Recall that all functions on a sphere can be written as spherical harmonics, meaning we can write the CMB temperature field $T(\hat{n})$ as

$$T(\hat{n}) = \sum_{\ell=0}^{\infty} \sum_{m=-\ell}^{\ell} a_{\ell m} Y_{\ell m}(\hat{n}),$$

where $\hat{n}$ is the direction on the sky, $a_{\ell m}$ is the coefficients of the spherical harmonics, and $Y_{\ell m}$ are the spherical harmonics. More commonly, we have written the temperature fluctuations

$$\Theta(x, \hat{p}, t) = \sum_{\ell=0}^{\infty} \sum_{m=-\ell}^{\ell} a_{\ell m} Y_{\ell m}.$$

Inflation predicts that initial perturbations, like Θ, is very close to a Gaussian random field. Consequently, the $a_{\ell m}$ will also be a Gaussian random field with soem variance C_ℓ. From this we can define the CMB power spectrum, given as the variance of the $a_{\ell m}$'s

$$C_\ell \equiv \langle |a_{\ell m}|^2 \rangle \quad \text{or} \quad C_\ell \delta_{\ell\ell'}\delta_{mm'} \equiv \langle a_{\ell m} a^*_{\ell' m'} \rangle, \qquad (80)$$

where the brackets denote an *ensemble mean*. We will get back to what this means. Notice that C_ℓ should in principle have two indices $C_{\ell m}$, but due to the assumption of an isotropic Universe, we must have full rotational invariance. Thus we average over m.

To get the power spectrum, we need to know the temperature today, $T(\hat{n}, x = 0)$, which we fortunately

"found" in Milestone 3 through the evolution of $\Theta_l(k,x)$. However, we will need at least $l = 1200$, which might take a lot of time to calculate. We will therefore do so called *line of sight integration*. The main idea is that instead of first expanding the temperature in multipoles as done in Eq.(62) and then solving the coupled equations, we directly integrate Eq.(61) and do the expansion in Eq.(62) at the end. The advantage of doing this is that instead of solving 1000 coupled ODE's, we can solve for any Θ_ℓ by only knowing Θ_0 and Θ_2 (and some other functions, it will soon be clear). Using that $\frac{d\tau}{d\eta} = -n_e\sigma_T a$ and re-ordering some terms we can rewrite Eq.(61) to

$$\dot{\Theta} + (ik\mu - \dot{\tau})\Theta = -\dot{\Phi} - ik\mu\Psi - \dot{\tau}\left[\Theta_0 + \mu v_b - \frac{1}{2}\mathcal{P}_2\Theta_2\right], \tag{81}$$

where $\dot{\Theta} \equiv \frac{d\Theta}{d\eta}$ and $\mathcal{P}_2(\mu) = \frac{3\mu^2-1}{2}$ is the second Legendre polynomial. We define the RHS as $\tilde{S}$, and the LHS can be re-written using integrating factors. We will soon keep redefining $\tilde{S}$, so wait a little bit for the final form of this function. This gives

$$\frac{d}{d\eta}\left(\Theta e^{ik\mu\eta - \tau}\right) = \tilde{S}e^{ik\mu\eta-\tau}.$$

Integrating both sides from $\eta_{\rm init}$ to η_0, we have

$$\Theta(\eta_0) = \Theta(\eta_{\rm init})e^{ik\mu(\eta_{\rm init}-\eta_0)-\tau(\eta_{\rm init})} + \int_{\eta_{\rm init}}^{\eta_0} d\eta \tilde{S}e^{ik\mu(\eta-\eta_0)-\tau},$$

where we used $\tau(\eta_0) = 0$. At early times, $\tau(\eta_{\rm init})$ will be really big, meaning the first term becomes negligible. Thus we can also replace $\eta_{\rm init}$ with 0, since any contribution $\eta < \eta_{\rm init}$ also becomes negligible. We thus have

$$\Theta(k,\mu,\eta_0) = \int_0^{\eta_0} d\eta \tilde{S}e^{ik\mu(\eta-\eta_0)-\tau(\eta)}. \tag{82}$$

This formula looks seemingly easy, but we still have a μ-dependence in $\tilde{S}$. The trick we will use to get rid of this is multiplying both sides with the Legendre-polynomial $\mathcal{P}_\ell(\mu)$, and integrate both sides. Using that

$$\Theta_\ell \equiv \frac{1}{(-i)^\ell}\int_{-1}^{1}\frac{d\mu}{2}\mathcal{P}_\ell\Theta(\mu)$$

and the relation between Legendre polynimials and spherical Bessel-functions $j_\ell(z)$

$$\int_{-1}^{1}\frac{d\mu}{2}\mathcal{P}_\ell(\mu)e^{ik\mu(\eta-\eta_0)} = \frac{1}{(-i)^\ell}j_\ell\left[k(\eta-\eta_0)\right].$$

We have to be careful though, since $\tilde{S}$ is μ-dependent. We can remove this μ-dependence by noting that we only multiply by polynomials in μ in the expression for $\tilde{S}$. Since we multiply $\tilde{S}$ with the exponential, we can replace $\mu \to \frac{1}{ik}\frac{d}{d\eta}$, and do integration by parts to move the derivative onto terms in $\tilde{S}$. This is best shown by example

$$\begin{aligned}
&-ik\int_0^{\eta_0} d\eta\, \Psi\mu e^{ik\mu(\eta-\eta_0)-\tau} \\
&= -\int_0^{\eta_0} d\eta\, \Psi e^{-\tau}\frac{d}{d\eta}de^{ik\mu(\eta-\eta_0)} \\
&= \int_0^{\eta_0} d\eta\, e^{ik\mu(\eta-\eta_0)}\frac{d}{d\eta}\left[\Psi e^{-\tau(\eta)}\right]
\end{aligned}$$

where the constant part from the integration by parts vanish. One term disappear since $\tau(0)$ is large, meaning $\Psi(0)e^{-\tau(0)} \approx 0$. We ignore $\Psi(\eta_0)e^{-\tau(\eta_0)}$ since this has no directional dependence (μ-dependence). Thus this only gives a non-zero contribution for $\ell = 0$, which only gives an unobservable shift in the monopole. Performing these steps on Eq.(82) and switching to integrating over x using $\frac{d\eta}{dx} = \frac{c}{\mathcal{H}}$, we get the equation

$$\Theta_\ell(k, x=0) = \int_{-\infty}^{0}\tilde{S}(k,x)j_\ell[k(\eta_0 - \eta(x))]dx, \tag{83}$$

where $j_\ell(z)$ is the spherical Bessel-functions (taking care of projecting a 3D-field onto a 2D spherical surface), and $\tilde{S}(k,x)$ is the source-function now defined as

$$\begin{aligned}
\tilde{S}(k,x) = &\tilde{g}\left[\Theta_0 + \Psi + \frac{1}{4}\Theta_2\right] + e^{-\tau}\left[\Psi' - \Phi'\right] \\
&- \frac{1}{ck}\frac{d}{dx}(\mathcal{H}\tilde{g}v_b) + \frac{3}{4c^2k^2}\frac{d}{dx}\left[\mathcal{H}\frac{d}{dx}(\mathcal{H}\tilde{g}\Theta_2)\right]
\end{aligned}$$

where all the quantities in the equations are known from previous Milestones. This is clearly a huge advantage, since we know only need to know Θ_0 and Θ_2 (+ some perturbations and functions that we already have) to get any Θ_ℓ, instead of solving 1000 coupled ODE's. The disadvantage is that we now need $j_\ell(z)$. The intuition of this approach is that looking at the CMB in a given direction, we add the contributions from the source function sourcing fluctuations in the CMB in that line of sight.

In the first term, we have a Θ_0 term which is the CMB monopole weighted by the visibility function (telling us how much we see the CMB), giving the monopole contribution to the fluctuations. The next is a contribution from Ψ, encoding that photons climb in and out of gravitational wells, giving fluctuating energy/temperature. The Θ_2 term is a small correction to the original Θ_0 term. The phenomena described by these three terms is often referred to as the "Sachs-Wolfe effect".
The second term is the "Integrated Sachs-Wolfe effect", describing the fact that the gravitational wells change while the photons still are inside them. The third term is a Doppler-effect term, and the fourth term comes from the angular dependence of Thompson scattering.

However, we are not quite done yet, as we still need to calculate C_ℓ. The expansion of Θ in spherical harmonics implies

$$\begin{aligned} a_{\ell m}(\vec{x},t) &= \int d\Omega_{\hat{p}} Y^*_{\ell m}(\hat{p})\Theta(\vec{x},\hat{p},t) \\ &= \int \frac{d^3k}{(2\pi)^3} e^{i\vec{k}\cdot\vec{x}} \int d\Omega_{\hat{p}} Y^*_{\ell m}(\hat{p})\Theta(\vec{k},\hat{p},t). \end{aligned}$$

Expanding Θ in multipoles further gives

$$\begin{aligned} a_{\ell m} = \sum_\ell (2\ell+1)(-i)^\ell \int \frac{d^3k}{(2\pi)^3} e^{i\vec{k}\cdot\vec{x}}. \\ \times \int d\Omega_{\hat{p}} Y^*_{\ell m}(\hat{p})\mathcal{P}_\ell(\mu)\Theta_\ell(\vec{k},t) \end{aligned}$$

Now, recall from Milestone 3 that in order to solve the equations numerically, we set $\Theta_\ell(\vec{k},t) = \Theta^{\text{code}}_\ell(k,t)\mathcal{R}_{\text{ini}}(\vec{k})$ where the initial value for the curvature perturbation $\mathcal{R}_{\text{ini}} \propto \Psi$ was set to unity. Now we must insert this back in to get the correct scaling. When we take the ensemble average over the $a_{\ell m}$'s, we will get

$$\left\langle \mathcal{R}_{\text{ini}}(\vec{k})\mathcal{R}^*_{\text{ini}}(\vec{k}')\right\rangle = (2\pi)^3\delta(\vec{k}-\vec{k}')P_{\text{prim.}}(k)$$

with

$$P_{\text{prim.}}(k) = \frac{2\pi^2}{k^3}A_s\left(\frac{k}{k_{\text{pivot}}}\right)^{n_s-1}$$

being the *primordial powerspectrum*, also known as the Harrison-Zel'dovich spectrum - which is predicted by most inflation models. The $n_s \sim 0.96$ is the spectral index of scalar perturbations, and k_{pivot} is some scale for which the amplitude is A_s. Using $k_{\text{pivot}} = 0.05/\text{Mpc}$ gives $A_s \sim 2\cdot 10^{-9}$. Then, by simple insertion and manipulation, we find

$$\begin{aligned} \langle a_{\ell m}a^*_{\ell' m'}\rangle = \sum_{\ell_1,\ell_2}(2\ell_1+1)(2\ell_2+1)(-i)^{\ell_1-\ell_2} \\ \times \int \frac{d^3k}{(2\pi)^3}\int d\Omega_{\hat{p}}d\Omega_{\hat{p}'}Y^*_{\ell m}(\hat{p})Y_{\ell' m'}(\hat{p}') \quad . \\ \cdot \mathcal{P}_{\ell_1}(\mu)\mathcal{P}_{\ell_2}(\mu')\Theta_{\ell_1}(k,t)\Theta_{\ell_2}(k,t)P_{\text{prim.}}(k) \end{aligned}$$

Next, using the identities

$$\begin{aligned} \int d\Omega_{\hat{p}}\mathcal{P}_\ell(\mu)Y^*_{\ell' m}(\hat{p}) = \delta_{\ell\ell'}\frac{4\pi}{2\ell+1}Y^*_{\ell m}(\hat{k}), \\ \int d\Omega_{\hat{k}}Y_{\ell m}(\hat{k})Y^*_{\ell m'}(\hat{k}) = \delta_{mm'}, \end{aligned}$$

we are left with

$$\langle a_{\ell m}a^*_{\ell' m'}\rangle = \delta_{\ell\ell'}\delta_{mm'}\frac{2}{\pi}\int dk\; k^2 P_{\text{prim.}}(k)|\Theta_\ell(k,t)|^2$$

with $\Theta_\ell = \Theta^{\text{code}}_\ell$ being what we calculate in our code. Comparing this to Eq.(80), we see that we must have

$$C_\ell = \frac{2}{\pi}\int k^2 P_{\text{prim.}}(k)\Theta^2_\ell(k)dk. \tag{84}$$

Substituting the primordial powerspectrum $P_{\text{prim.}}(k)$ gives the final equation as

$$C_\ell = 4\pi\int_0^\infty A_s\left(\frac{k}{k_{\text{pivot}}}\right)^{n_s-1}\Theta^2_\ell(k)\frac{dk}{k}, \tag{85}$$

According to [7], one can find that when the Sachs-Wolfe term is dominating, we have

$$C^{\text{SW}}_\ell \overset{\propto}{\sim} \frac{\Gamma\left(\ell+\frac{n_s}{2}-\frac{1}{2}\right)\Gamma\left(3-n_s\right)}{\Gamma\left(\ell+\frac{5}{2}-\frac{n_s}{2}\right)\Gamma^2\left(2-\frac{n_s}{2}\right)}, \tag{86}$$

where Γ is the gamma-function. With $n_s \approx 1$, we get by using $\Gamma(z+1) = z\Gamma(z)$ that $\ell(\ell+1)C_\ell = \text{constant}$. Lastly, we will define the matter power spectrum, given as

$$P(k,x) = |\Delta_M(k,x)|^2 P_{\text{prim.}}(k), \tag{87}$$

where Δ_M is defined as

$$\Delta_M(k,x) \equiv \frac{c^2k^2\Phi(k,x)}{\frac{3}{2}\Omega_{M0}a^{-1}H_0^2}. \tag{88}$$

4.1.3. Cosmic variance

The power spetrum defined in Eq.(80) is defined as an average over the squared coefficients of the spherical harmonics. Another way to put this is that C_ℓ is the variance of $a_{\ell m}$. The angled brackets denote an ensemble average, meaning an average over many possible realizations of our Universe.
Since m ranges between $-\ell, \ell$, we have $2\ell+1$ values for m. Thus we can estimate the power spectrum C_ℓ after measuring $a_{\ell m}$ as

$$\hat{C}_\ell = \frac{1}{2\ell+1}\sum_{m=-\ell}^{\ell}|a_{\ell m}|^2.$$

However, we only have one Universe to make measurements in. This is where the *ergodic hypothesis* comes in: *"The ensemble average is equal to a spatial average taken over one realisation of the field"*, meaning that as long as we have enough modes, the mean of these will be the same as the ensemble average. This means that for large ℓ-values, we have a enough m's to properly estimate C_ℓ. However, for low ℓ-values, we have very few values for m to estimate C_ℓ, giving a lot of uncertainty. This uncertainty is called *cosmic variance*, where we have a fundamental uncertainty in C_ℓ we can't get around due to only having one Universe to make measurements. Since the $a_{\ell m}$'s are independent Gaussian random variables, their squared sum ($\hat{C}_\ell$) is distributed according to the χ^2-distribution. Thus the cosmic variance is given as

$$\frac{\text{Var}(C_\ell)}{C_\ell^2} = \frac{2}{2\ell+1}.$$

Note that this is defined slightly different than the regular variance. A detailed derivation can be found in [7], where it also becomes apparent that we have ignored atmospheric/instrumental noise.

4.2. Implementation, numerical methods and tests

First off, we go back to Milestone 3 and implement the source function $\tilde{S}$, as this is dependent on quantities calculated in this Milestone. Since this function depends on k, x, we make a 2D spline of this quantity.

Next, we need to implement the Bessel-functions. Looking up these functions, one find that these look like damped oscillations, meaning we have to be careful with sampling enough points from these. Bessel-functions have period $\lambda \approx 2\pi$, meaning sampling n points in a period means $\Delta x = \frac{\lambda}{n} \approx \frac{2\pi}{n}$. Since the argument of the Bessel-function is $z = k(\eta_0 - \eta)$ with $\eta \leq \eta_0$ for $x \leq 0$, we need $z \in [0,\ k\eta_0 \sim 3000]$. Doing some testing, we find that $\Delta x = 2\pi/n_{\text{bessel}}$, $n_{\text{bessel}} \sim 16$ works fine, meaning sampling with ~ 16 points per oscillation. Instead of making a reference to the Bessel-functions each time we need them, we choose to spline them to make more efficient code.

Running a quick test to check that we implemented the Bessel-splines correctly, we choose $\ell_{\text{test}} = \{6,\ 100,\ 200,\ 500,\ 1000\}$ and plot the Bessel-functions. We will in general use these ℓ-values to plot other quantities as well. The result can be seen in Fig.(21), and looks promising.

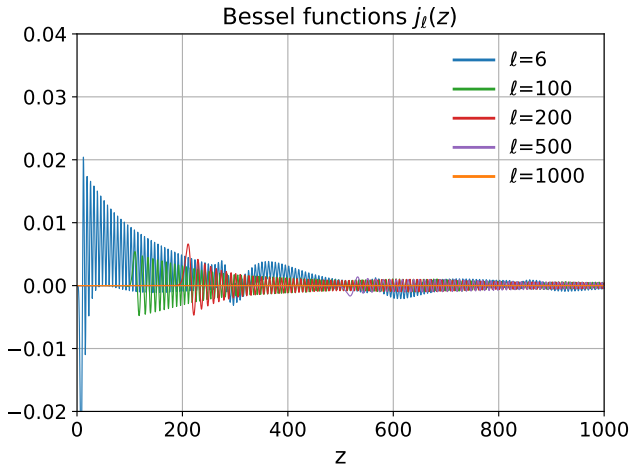

FIG. 21: Plot of the spherical Bessel-functions for some given values of ℓ. The z in the plot is not the redshift, but a generic input to the Bessel-function.

Now we will do the line of sight integration for each ℓ to solve for Θ_ℓ. We choose to use the values

$$\begin{aligned}\ell = \{&2, 3, 4, 5, 6, 7, 8, 10, 12, 15, 20, 25, 30,\\ &40, 50, 60, 70, 80, 90, 100, 120, 140, 160,\\ &180, 200, 225, 250, 275, 300, 350, 400, 450,\\ &500, 550, 600, 650, 700, 750, 800, 850, 900, 950,\\ &1000, 1050, 1100, 1150, 1200, 1250, 1300, 1350,\\ &1400, 1450, 1500, 1550, 1600, 1650, 1700, 1750,\\ &1800, 1850, 1900, 1950, 2000\},\end{aligned}$$

where we have omitted the $\ell = 0, 1$ values as $\ell = 0$ only represents the average temperature, and $\ell = 1$ represents the effects of an observer moving wrt. the CMB. Making a linspace of the k-values with $\Delta k = \frac{2\pi}{\eta_0 n}$, $n \sim 100$, we straightforwardly solve for Θ_ℓ and make splines. Performing the integral, we will simply use a trapezoidal integral, since this is fairly easy to implement. Alternatively, one could use the ODESolver from GSL. For the line of sight integration, we will sample $\Delta x = 2\pi/n_{\text{los}}$ with $n_{\text{los}} \sim 100$ in the trapezoid integral. Also notice that according to Eq.(83), we are supposed to integrate from $-\infty$, which is numerically impossible. By plotting the integrand $\tilde{S}(k, x) j_\ell\left[k(\eta_0 - \eta)\right]$, one can see that integrating from $x = -8$ is sufficient.

Next, we need to solve for the power spectrum. We choose to use logarithmically spaced k-values, but this gives some additional challenge. Using Eq.(85) and rewriting $\frac{dk}{k} = d(\ln(k))$, we essentially have the ODE

$$\frac{dC_\ell}{d\ln(k)} = 4\pi A_s \left(\frac{k}{k_{\text{pivot}}}\right)^{n_s - 1} \Theta_\ell^2(k).$$

Writing it like this allows us to use logarithmically spaced k-values by making a linearly spaced array, starting at $\ln(k_{\text{start}})$ and ending at $\ln(k_{\text{end}})$. This gives $\Delta k = (\ln(k_{\text{end}}) - \ln(k_{\text{start}}))/N$ with $\eta_0 \Delta k = \frac{2\pi}{n_{\text{ps}}}$, $n_{\text{ps}} \sim 100$. Then we just exponentiate $k_{\text{val}} = \exp(k[i])$ when looping over k's to evaluate the integral, giving the log-spacing between values as we wanted. To solve the integral, we integrate using the trapezoidal integral.

When integrating to solve for C_ℓ, the main contribution comes from the transfer function Θ_ℓ. Therefore we have plotted the transfer-function, alongside with the dominating part of the integrand in C_ℓ. These might be useful for later discussions. Also notice that we plotted these as functions of scale $k\eta_0$, as this provides an intuitive picture. We can write $k\eta_0 \sim \frac{\eta_0}{\lambda}$, where λ is the length scale we are working on. Thus, $k\eta_0 = 10^3$ means $\lambda \sim \eta_0 \cdot 10^{-3}$, meaning we are looking at scales that are one thousandth of the observable Universe.

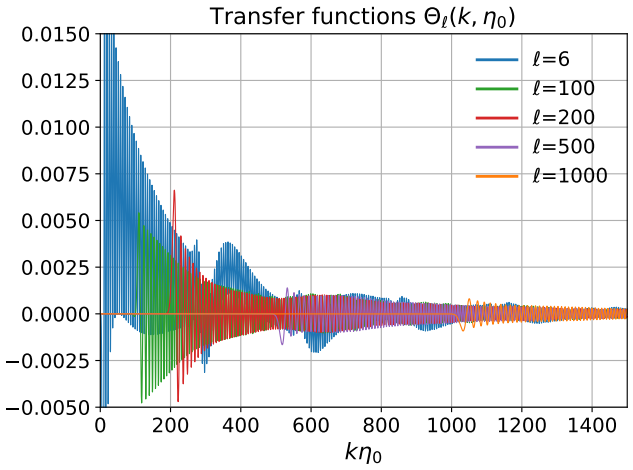

FIG. 22: Plot of the transfer functions/multipoles Θ_ℓ.

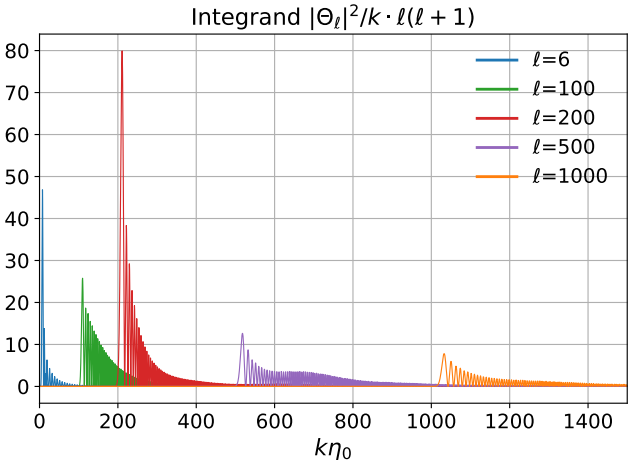

FIG. 23: Plot of the essential part of the C_ℓ integrand, effectively acting as an on/off switch. The integrand is plotted in units $\ell(\ell+1)$, meaning you should roughly read of graph by dividing ℓ^2.

4.2.1. Calculating the CMB map

This section would be short, but hopefully helpful for those who want to replicate this. To calculate the CMB map, we use the "healpy" library offered in Python. To get the CMB map, you would want to set a random seed by using "numpy" with "np.random.seed(seed)". We used seed=5220. Then we generate the CMB map from C_ℓ by calling "cmb_map=hp.synfast(C_ell, nside=nside, lmax=lmax, mmax=lmax)", where "nside" is the resolution of the map. We used nside=2^{10}. Lastly, we want to project the map. To do this, we used "hp.mollview(cmb_map)", which gives the final map. For more details, see the documentation linked.

4.3. Results and discussion

In Fig.(24), we can see a plot of the matter power spectrum. The dashed line k_{eq} represents radiation-matter equality, which we find to be approximately at the maxima of the matter power spectrum. The errorbars represent data from Galaxy surveys (SDSS DR7 LRG) [3] and WMAP+ACT [4]. The figure shows some devations between theoretical predictions and observed data, which might be due to ignoring neutrinos and polarization.

First, we should discuss what the matter power spectrum represents. The distribution of matter in the Universe is not uniform, and exactly how much matter clusters on various scales is statistically described by the two-point correlation function $\xi(r_{ij}) = \langle\delta(\vec{x}_i)\delta(\vec{x}_j)\rangle$. The two-point correlation function gives the probability of finding a clump of matter at a distance r from another clump of matter. The power spectrum is the Fourier-transformed quantity of $\xi(r)$ - as described in the Theory section, then telling us *how much structure* there is on various scales by decomposing the probability into characteristic lengths k. The amplitude of the power spectrum then describes to which degree each characteristic length contributes to the total probability. In Fig.(13a), modes on the right side represents small scales, while the left side represents large scales. The smaller the scale is, the earlier in time it enters the horizon. Comparing to the k_{eq}-line, this means that to the right of k_{eq} is during radiation-domination, while to the left of k_{eq} is during matter-domination (matter-DE equality happens even further to the left, outside the plot).

From Eq.(87) we can see that $k^3P(k,0) \propto \Delta_M^2(k,0)$. During matter domination, we then get from Eq.(88) that $\Delta^2 \propto k^4$, meaning that the matter power spectrum goes as $P(k,0) \propto k$. This becomes apparent in Fig.(24), where we can see the linear growth to the left of k_{eq}.. This is a direct consequence of the initial conditions imposed by inflation, and the power spectrum not being evolved at the largest scales.
One can show that the gauge invariant density $\Delta_M = \delta - \frac{3\mathcal{H}}{k}v$[9]

Radiation era:

- Mode outside horizon: $\Delta_M \propto a^2$
- Mode inside horizon: $\Delta_M \propto \ln(a)$

Matter era:

- Mode outside horizon: $\Delta_M \propto a$
- Mode inside horizon: $\Delta_M \propto a$

Now, we turn back to Milestone 3. Looking at Fig.(19), we see that the small-scale mode ($k = 0.1$/Mpc) enters the horizon during radiation-domination, before

radiation-matter equality. During radiation-domination the potential decays, making the growth of the density-perturbation seen in Fig.(13a) retarded from $x \approx -9$ until matter-domination, called the *Meszaros-effect*. This becomes even more prominent plotting at larger modes. More specifically, for for sub-horizon modes ($\Delta_M \approx \delta$) we have $\delta \propto \ln(a)$ during radiation-domination (while modes outside the horizon $\delta \propto a^2$), which is slower than the expansion of the Universe. This leads to the density being suppressed during radiation domination. The earlier the density-mode enters the horizon, the more suppressed it gets from the logarithmic growth. Therefore, the power-spectrum will be decreasing on small scales, instead of following the linear growth from the larger scales. One can show that $\Delta^2 =$ constant. on these scales, giving $P(k, 0) \propto k^{-3}$ [7], which also is apparent in Fig.(24).

This leads to the realization that there will be a peak in the power-spectrum, but where? Since the overdensities are suppressed during radiation-domination, the maxima should occur at radiation-matter equality k_{eq}, as this is the mode that has spent the least time in radiation-domination, thus being the least suppressed. This peak gives a theoretical limit for how large cosmological structures can get. Due to numerical inaccuracies and plotting on a sensitive scale, the $k_{\text{eq.}}$ line in Fig.(24) is not really the true maxima, but close. Using the true maxima of the power-spectrum gives an upper scale-limit of $\lambda \approx 486\,\text{Mpc} = 1.62\,\text{Gly}$, while using the value in the plot gives $\lambda \approx 605\,\text{Mpc} = 2.0\,\text{Gly}$.

We should also comment on the small wobbling in the matter power spectrum seen in radiation domination. These can be explained by the baryon acoustic oscillations (BAO) discussed in Milestone 3. The fluctuations in Fig.(24) are not as prominent as in Fig.(25), since the baryons make up less of the total matter than dark matter does, leading to the effect being suppressed.

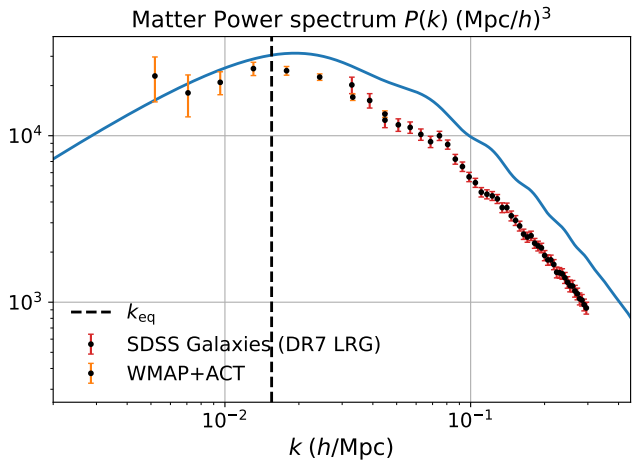

FIG. 24: The theoretical prediction of the matter power spectrum. The yellow errorbars are from WMAP+ACT [4], and the red errorbars from Galaxy surveys (SDSS DR7 LRG) [3]. The dashed line k_{eq} represents radiation-matter equality. To compare the k-values in this plot with that of Fig.(13a), one should multiply the value read off in this figure by $h = 0.67$.

In Fig.(25), we see the plot of the CMB power spectrum today. The green band represents the cosmic variance, and the errorbars represent data from Planck 2018 [1]. The figure shows some deviation from the observed values, which is due to us ignoring the effects of neutrinos and polarization. This is mostly visible in the region of high ℓ-values, since we have a large statistical uncertainty in observational data at small ℓ-values. Further, we will divide the discussion into two parts: low ℓ-values, and large ℓ-values.

Small ℓ-values: In Fig.(25) we can see that for small ℓ-values i.e. large scales, the power spectrum appears almost flat. These scales corresponds to the scales in Milestone 3 that entered the horizon after recombination. Since these scales entered after recombination, the anisotropies are not affected by any microphysics - only $\Theta_0 + \Psi$ evaluated at recombination contribute to anisotropies. Adding Θ_2, this corresponds to the Sachs-Wolfe (SW) term from the source function $\tilde{S}$. Since the SW term is multiplied by the visibility function $\tilde{g}$, it is apparent from Fig.(12) that it contributes only during recombination.

The given contribution to C_ℓ is also seen in Fig.(23), where for large scales (e.g. $\ell = 6$), the integrand is zero at large $k\eta_0$, and non-zero at small $k\eta_0$. This means that only large-scale anisotropies contribute to low ℓ's. We can also see that the flat behaviour is described by the approximation in Eq.(86), telling us that $\ell(\ell+1)C_\ell =$ const. However, the other contributions in the source-function are not unpresent, meaning we should not expect $\ell(\ell+1)C_\ell$ to be completely

flat. The Integrated Sachs-Wolfe effect (ISW) plays a role, telling us potentials that change after recombination contribute. Given that the potential changes at η_c with scales $k\eta_c > 1$ being affected, scales at $\ell > (\eta_c - \eta_0)/\eta_c$ would be affected by ISW as the Bessel-function peaks at $\ell \sim k(\eta_0 - \eta_c)$[7]. In our case, this would be about $\ell > (15000 - 1500)/1500 = 9$. This "flat" region is often referred to as the "Sachs-Wolfe plateau", and approximate flatness seems to be maintained until $\ell \approx 20$ in Fig.(25).

As a result of large scales entering the horizon after recombination, large scale perturbations will experience small fluctuations from the initial state - and therefore the power spectrum resembles the initial condition given by inflation. This is not too surprising, as causal physics can not affect perturbations with modes larger than the horizon.

We should also comment the cosmic variance. As previously explained, these are expected to be larger at the low ℓ's, due to only having one Universe to make measurements. This is also reflected in large errorbars from the Planck data, which comes from looking at large regions of the sky - giving few sample points to give accurate statistical estimates of C_ℓ. In Fig.(25) we can see a small dip in data around $\ell \approx 23$, making a discrepancy between theory and data. Since the errorbars overlap with the cosmic variance, we could still have power spectrums that fall into the dip - still being inside both the errorbar and cosmic variance. The statistical nature of the spectrum thus suggests that this might be a statistical fluke.

Large ℓ-values: Large ℓ-values are characterized by the first large peak and the following. The peaks seen in Fig.(25) comes from baryon acoustic oscillations discussed in Milestone 3. These acoustic waves comes from interplay between gravitational forces from baryons and dark matter and radiation pressure from photons, resulting in propagating waves of photon-baryon plasma. The first compression of the photo-baryon plasma corresponds to the first peak in Fig.(25). At early times, this peak was at a much higher ℓ-value (at a smaller scale). As the photon-baryon wave propagates in time, the peak travels from right to left in Fig.(25), since it moves from smaller to larger scales. Then at recombination, photons decouple from baryons, leaving them behind. This means that the peak stops moving, and therefore the first peak also represents when recombination happened. In our case, Fig.(25) tells us recombination happened at $\ell \sim 200$. Since the wave-production follows an oscillatory motion, each peak corresponds to a compression/decompression (since we use $|\Theta_\ell|^2$). Counting from 1, each odd peak corresponds to a compression, while each even peak corresponds to a decompression.

Going to even larger ℓ-values (smaller scales) we see that the acoustic oscillations decrease rapidly, looking like a tail for the CMB spectrum. Previously, we have described photons and baryons as tightly coupled, but this is only an approximation. Before recombination, photons scattered off free electrons/protons, and was thus "trapped". This leads to the photon having a small mean free path, and the effect is that the diffusing photons travels from hot regions of space to cold regions (diffusion) - effectively smoothing out temperature fluctuations and making the CMB more uniform. The effect is damping caused by diffusion. Let us try to roughly discuss this a bit more qualitatively, without introducing too much new stuff: Imagine that the photons have diffusion length (the average distance that a photon travel before recombining) $D = \frac{2\pi}{k_D}$. Thinking of scattering photons as random walks we can use the diffusion equation $\dot{f} = F\nabla^2 f$, which describes macroscopic behavior of many micro-particles in random motion. $F = \frac{D^2}{4\pi^2 t}$ is the diffusion coefficient. Taking the Fourier-transform of the diffusion-equation, one obtains $f \propto \exp(-k^2/k_D^2)$ which washes away modes around the scale k_D. In Fig.(25), one would see the diffusion damping occur around $\ell \sim 900$. From the relation above, we also roughly see that a small diffusion length D makes the tail decrease slower, while large diffusion length makes the tail decrease faster. During recombination the photons get a larger mean free path due to reduction of electron density, and thus larger diffusion length - giving the diffusion-damped tail we observe in Fig.(25).

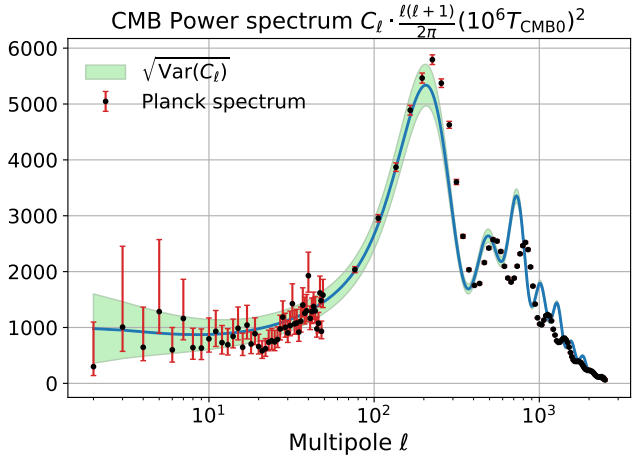

FIG. 25: The theoretical prediction of the power spectrum today plotted in units $\frac{2\pi}{\ell(\ell+1)}(1 +^6 T_{\mathrm{CMB0}}))\,[\mu\mathrm{K}^2]$. The errorbars are data from Planck 2018 [1], and the green band represents the cosmic standard deviation $\sigma(C_\ell) = \sqrt{\mathrm{Var}(C_\ell)}$.

The final result of this report is a rendering of the CMB seen in Fig.(26), and no document calculating the power spectrum would be complete without it. There is not too much to comment on this, other than the map looking slightly sharper than observed data, due to smoothing of the instrumental beams. This can be simulated by smoothing the map using a Gaussian beam in healpy.

4.4. Conclusions

We found that the matter power spectrum increases during matter domination (large scales) due to not being evolved, giving the shape of the initial conditions. This gives the power-spectrum $P(k) \propto k$ before radiation-matter equality. In radiation-domination, we found that modes entering the horizon experiences suppression from logarithmic growth, also known as the Meszaros-effect, leading to the matter power spectrum decreasing as $P(k) \propto k^{-3}$ before radiation-matter equality. This led us to the realization of the matter-spectrum having a peak, which we concluded to be in the radiation-matter equality scale $k_{\text{eq.}}$. We also found the an upper-bound of structure scales at $\lambda \approx 486\,\text{Mpc} = 1.62\,\text{Gly}$.

For the CMB power spectrum, we found that large scales gives a flat spectrum, also known as the Sachs-Wolfe plateau. Again, due to large scales not evolving, the early CMB spectrum resembles the initial conditions imposed by inflation. We estimated the flatness of the spectrum to last until $\ell > 9$, where we get a noticable contribution from the Integrated Sachs-Wolfe effect. Seemingly, the flatness is maintained until $\ell \approx 20$. We also concluded that the first peak in the spectrum comes from the first compression of baryon acoustic waves, while the position of the peak along the x-axis represents where recombination happens. The following peaks corresponds to decompression/compression. Next last we discussed the damping tail, caused by diffusion damping on very small scales. We found that the tail decrease faster if the diffusion length D of the diffusing photons increase, and the tail decrease slower if the diffusion length increase. At last we commented the cosmic variance of the CMB spectrum, coming from the intrinsic statistical uncertainty of only having one Universe to make measurements. Having less statistical data to make estimations of C_ℓ at large scales, we have a greater uncertainty at small ℓ's in the power spectrum. This can be connected to the large size of the errorbars from the Planck data, also due to having a low set of data-points to give estimations of C_ℓ on large scales as we then observe larger regions of the sky.

5. SUMMARY

During this project, we have discovered various results about the Universe. We shall now try to summarize these.

In Milestone 1, we calculated the **background cosmology** of the Universe. We used the cosmological principle to arrive at a Friedmann-Robertson-Walker Universe, and used the Einstein-equations to derive the Friedmann-equations. Further, we then defined the Hubble factor, and solved for the evolution of the cosmological background parameters. We found that the acceleration of the Universe happened at $\Omega_\Lambda \approx \frac{1}{3}$, and that the Universe is $t = 13.86\,\text{Gyr}$ old. We also used a MCMC algorithm to compare our theoretical model to supernovadata from [2], and found that a flat universe must have densities $\Omega_\text{M} \sim 0.23 - 0.33$ and $\Omega_\Lambda \sim 0.66 - 0.76$.

In Milestone 2, we calculated the **recombination history** of the Universe. This epoch is important, as this is where the CMB photons become visible. Due to the expansion of the Universe, photons redshift and become less energetic - making the Universe colder. This causes the photons to no longer ionize hydrogen, allowing free electrons to bind to protons - forming neutral matter. This means recombination does not happen instantaneously, but over a given period of time. However, there exists a point in time where it was most likely for the photon to last scatter with the free electrons - the event of last scattering. We found this event to happen at time $t = 0.37801\,\text{Myr}$. We also saw that not all free electrons ended up forming neutral matter, leaving a freeze-out abundance $X_e(x = 0) = 2.02 \cdot 10^{-4}$.

In Milestone 3 we realized that the Universe is not entirely flat, as we until this point had assumed. This led us to doing **perturbations** on several cosmological parameters - more specifically linear perturbation theory, leading to a whole series of interesting physics. One of these was the *baryon acoustic oscillations*, encapsulating the interplay between pressure forces from radiation and gravitation from growing overdensities. This led to an oscillatory behaviour of the photon-baryon plasma before recombination due to compression and decompression caused by this interplay. Then when recombination happened, photons were no longer coupled to baryons, leaving behind shells of overdense regions of matter - causing the formation of cosmological structures. This only affected modes that entered the horizon before recombination.

Finally, in Milestone 4, we arrived at the **CMB power spectrum**. We realized that solving the coupled ODE's from Milestone 3 is hard work, and developed a new technique for evaluating photon multipoles. From the matter power spectrum, we arrived at a theoretical limit for the size of structures in the Universe, found as $\lambda \approx 486\,\text{Mpc} = 1.62\,\text{Gly}$. We discussed the intrinsic uncertainty of the power spectrum, caused by only having one Universe to make measurements in - known as comsic variance. We found that the first peak in the CMB power spectrum corresponds to when recombination happened.

For further work, we could include neutrinos, polarization, and matter heavier than hydrogen in our model to make more accurate predictions. We could also do perturbation theory beyond the first order, which would indeed make the model more complicated to solve.

ACKNOWLEDGMENTS

I want to give a special thanks to Edvard Rørnes, who has been a great companion during the project, offering both interesting and insightful discussions. I would also thank Hans Winther and David Mota for making this an educational experience.

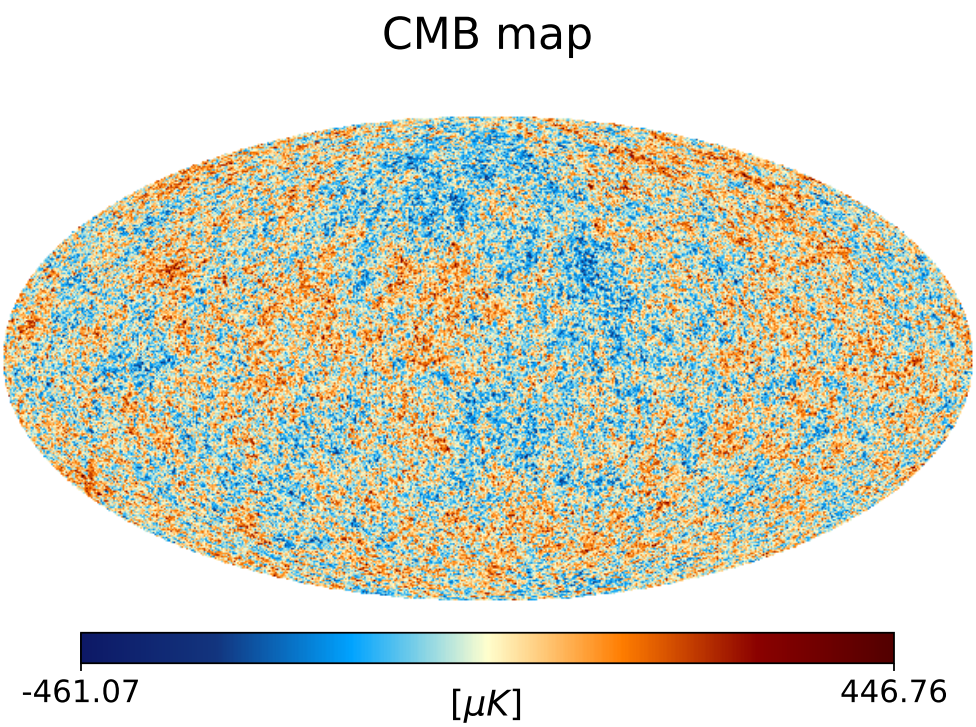

FIG. 26: The Cosmic Microwave Background.

[1] N. Aghanim, Y. Akrami, *et. al.*, *Planck2018 results: VI. cosmological parameters*, *Astronomy amp; Astrophysics* **641** (2020) A6.
[2] SDSS: M. Betoule *et. al.*, *Improved cosmological constraints from a joint analysis of the SDSS-II and SNLS supernova samples*, *Astron. Astrophys.* **568** (2014) A22, [arXiv:1401.4064].
[3] B. A. Reid, W. J. Percival, *et. al.*, *Cosmological constraints from the clustering of the sloan digital sky survey dr7 luminous red galaxies*, *Monthly Notices of the Royal Astronomical Society* (2010).
[4] R. Hlozek, J. Dunkley, *et. al.*, *The atacama cosmology telescope: A measurement of the primordial power spectrum*, *The Astrophysical Journal* **749** (2012) 90.
[5] H. A. Winther, H. K. Eriksen, O. Elgaroy, D. F. Mota, and H. Ihle, "Cosmology II." https://cmb.wintherscoming.no/, 2024. Accessed on May 20, 2024.
[6] L. Senatore, S. Tassev, and M. Zaldarriaga, *Cosmological Perturbations at Second Order and Recombination Perturbed*, *JCAP* **08** (2009) 031, [arXiv:0812.3652].
[7] S. Dodelson, *Modern Cosmology*. Academic Press, Amsterdam, 2003.
[8] P. Callin, *How to calculate the CMB spectrum*, astro-ph/0606683.
[9] P. Meszaros, *The behaviour of point masses in an expanding cosmological substratum*, *Astron. Astrophys.* **37** (1974) 225–228.